Cancer Cell

Article

Early immune pressure initiated by tissue-resident memory T cells sculpts tumor evolution in non-small cell lung cancer

Graphical abstract

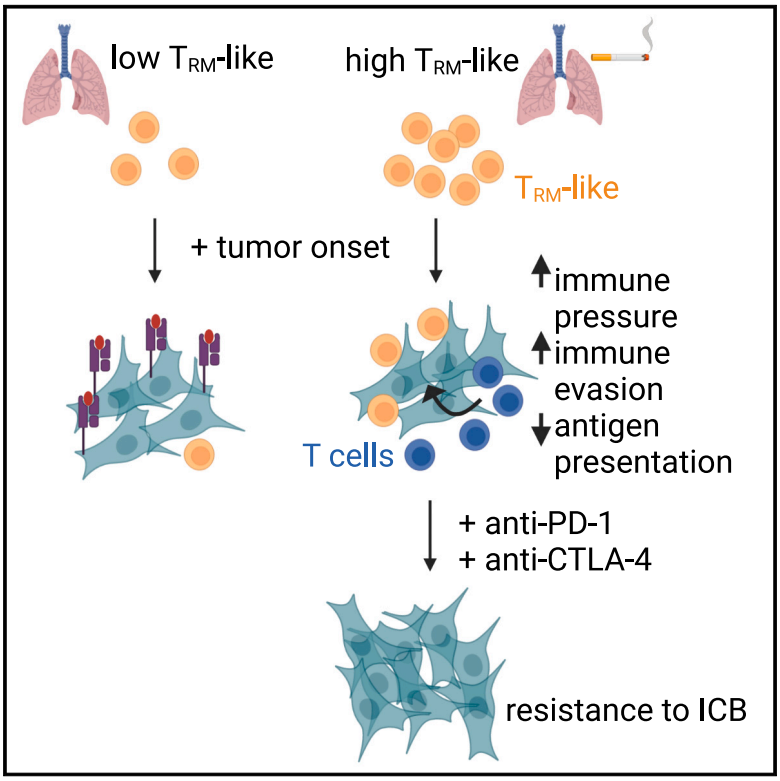

Highlights

- Activated T_{RM}-like cells are enriched in the lungs of ever-smoker individuals
- T_{RM}-like cells of any specificity present before tumor growth accelerate immune evasion
- Tumors grown in T_{RM} cell-rich environments become resistant to immune checkpoint blockade

Authors

Clare E. Weeden, Velimir Gayevskiy, Claire Marceaux, ..., Terence P. Speed, Daniel H.D. Gray, Marie-Liesse Asselin-Labat

Correspondence

dgray@wehi.edu.au (D.H.D.G.), labat@wehi.edu.au (M.-L.A.-L.)

In brief

Weeden et al. find that ever-smoker lungs have greater activation of T cells with a tissue-resident memory phenotype (T_{RM}). Lung tumors growing in T_{RM} cell-rich environments develop immune evasion, leading to immune checkpoint therapy resistance. These findings identify that the "soil" in which tumors are grown has lasting effects on tumor immunogenicity and therapy response.

Weeden et al., 2023, Cancer Cell *41*, 837–852
May 8, 2023
https://doi.org/10.1016/j.ccell.2023.03.019

CellPress

Cancer Cell

CellPress
OPEN ACCESS

Article

Early immune pressure initiated by tissue-resident memory T cells sculpts tumor evolution in non-small cell lung cancer

Clare E. Weeden,[1,6] Velimir Gayevskiy,[1,6] Claire Marceaux,[1,6] Daniel Batey,[1] Tania Tan,[2] Kenta Yokote,[1] Nina Tubau Ribera,[3] Allison Clatch,[11] Susan Christo,[11] Charis E. Teh,[2,6] Andrew J. Mitchell,[8] Marie Trussart,[4] Lucille C. Rankin,[2,6] Andreas Obers,[11] Jackson A. McDonald,[5,6] Kate D. Sutherland,[5,6] Varun J. Sharma,[9,15,16] Graham Starkey,[9,15] Rohit D'Costa,[18,19] Phillip Antippa,[9,12] Tracy Leong,[1,6,13] Daniel Steinfort,[10,12] Louis Irving,[10,12] Charles Swanton,[20,21,22] Claire L. Gordon,[11,14,17] Laura K. Mackay,[11] Terence P. Speed,[4,7] Daniel H.D. Gray,[2,6,23,*] and Marie-Liesse Asselin-Labat[1,6,23,24,*]

[1]Personalised Oncology Division, Walter and Eliza Hall Institute of Medical Research, Parkville, VIC, Australia
[2]Immunology Division, Walter and Eliza Hall Institute of Medical Research, Parkville, VIC, Australia
[3]Advanced Technology and Biology Division, Walter and Eliza Hall Institute of Medical Research, Parkville, VIC, Australia
[4]Bioinformatics Division, Walter and Eliza Hall Institute of Medical Research, Parkville, VIC, Australia
[5]ACRF Stem Cells and Cancer Division, Walter and Eliza Hall Institute of Medical Research, Parkville, VIC, Australia
[6]Department of Medical Biology, the University of Melbourne, Parkville, VIC, Australia
[7]School of Mathematics and Statistics, the University of Melbourne, Parkville, VIC, Australia
[8]Materials Characterisation and Fabrication Platform, Department of Chemical Engineering, the University of Melbourne, Parkville, VIC, Australia
[9]Department of Surgery, University of Melbourne, Parkville, VIC, Australia
[10]Department of Medicine, the University of Melbourne, Parkville, VIC, Australia
[11]Department of Microbiology and Immunology, the University of Melbourne, at the Peter Doherty Institute for Infection and Immunity, Parkville, VIC, Australia
[12]The Royal Melbourne Hospital, Parkville, VIC, Australia
[13]Department of Respiratory and Sleep Medicine, Austin Health, Heidelberg, VIC, Australia
[14]Department of Infectious Diseases, Austin Health, Heidelberg, VIC, Australia
[15]Liver and Intestinal Transplant Unit, Austin Health, Heidelberg, VIC, Australia
[16]Department of Cardiothoracic Surgery, Austin Health, Heidelberg, VIC, Australia
[17]North Eastern Public Health Unit, Austin Health, Heidelberg, VIC, Australia
[18]DonateLife Victoria, Carlton, VIC, Australia
[19]Department of Intensive Care Medicine, Melbourne Health, Melbourne, VIC, Australia
[20]Cancer Research UK Lung Cancer Centre of Excellence, University College London Cancer Institute, London, UK
[21]Cancer Evolution and Genome Instability Laboratory, Francis Crick Institute, London, UK
[22]Department of Oncology, University College London Hospitals, London, UK
[23]These authors contributed equally
[24]Lead contact
*Correspondence: dgray@wehi.edu.au (D.H.D.G.), labat@wehi.edu.au (M.-L.A.-L.)
https://doi.org/10.1016/j.ccell.2023.03.019

SUMMARY

Tissue-resident memory T (T_{RM}) cells provide immune defense against local infection and can inhibit cancer progression. However, it is unclear to what extent chronic inflammation impacts T_{RM} activation and whether T_{RM} cells existing in tissues before tumor onset influence cancer evolution in humans. We performed deep profiling of healthy lungs and lung cancers in never-smokers (NSs) and ever-smokers (ESs), finding evidence of enhanced immunosurveillance by cells with a T_{RM}-like phenotype in ES lungs. In preclinical models, tumor-specific or bystander T_{RM}-like cells present prior to tumor onset boosted immune cell recruitment, causing tumor immune evasion through loss of MHC class I protein expression and resistance to immune checkpoint inhibitors. In humans, only tumors arising in ES patients underwent clonal immune evasion, unrelated to tobacco-associated mutagenic signatures or oncogenic drivers. These data demonstrate that enhanced T_{RM}-like activity prior to tumor development shapes the evolution of tumor immunogenicity and can impact immunotherapy outcomes.

INTRODUCTION

Carcinomas evolve from small expansions of transformed epithelial cells into pre-invasive lesions and eventually into overt malignancies. These cells accumulate mutations that can create neoantigens, novel peptides that may provoke an adaptive immune response.[1] The adaptive immune system protects the host from malignant growth by eliminating tumor cells, yet it also exerts selective pressure upon nascent cancers to evade immune predation.[2] Tissue-resident memory T (T_{RM}) cells provide rapid recall responses to tissue-specific infections and have also been shown to promote cancer-immune equilibrium.[3] How early immunosurveillance by *in situ* T_{RM} cells might influence immune cell recruitment to developing tumors, and the impact upon the evolution of tumor immunogenicity is unknown. Lung adenocarcinoma (LUAD) represents an ideal scenario to address these questions due to its prevalence in both never-smoker (NS) and ever-smoker (ES, current- and ex-smoker) patients, where tobacco smoking enhances both the accumulation of DNA alterations in lung epithelial cells[4,5] and chronic inflammation within the lung.[6] In these two patient groups, we can assess the impact of pre-existing chronic inflammation and tumor mutational burden (TMB) upon tumor progression from pre-invasive to invasive late-stage disease.

The genomic drivers of NS LUAD are distinct from those in patients with a history of cigarette smoking. Alterations in *EGFR*, *ROS1*, and *ALK* are more common in NS tumors, while *KRAS*, *TP53*, *KEAP1*, *BRAF*, and *JAK2/3* alterations are characteristic of ES tumors.[7] These differences guide distinct clinical treatments with targeted kinase inhibitors deployed according to genetic testing.[8] NS patients with lung cancer respond poorly to immune checkpoint inhibitors compared with ES patients.[9] It has been suggested that tumor cell-intrinsic factors such as lower TMB and lower expression of PD-L1 account for this reduced sensitivity.[10–12] Yet, other smoking-induced factors may influence checkpoint immunotherapy responses. We reasoned that T_{RM} cell abundance and activation state before tumor onset may differentially influence tumor evolution in ES and NS patients and could be decisive in treatment response.

T_{RM} cells reside in tissues and provide tissue-specific local immunity.[13,14] They have been extensively studied within the murine lung in response to infections such as influenza[15] and have recently been identified as the dominant T cell population within healthy adult human lung.[16,17] Cells with a T_{RM} phenotype can be defined in humans by expression of the memory marker CD45RO, the absence of lymph node homing molecules (i.e., CCR7), surface expression of CD69, and in some instances, the αE integrin CD103[18]; however, it is not always possible to establish whether these are truly memory cells and so are referred to as T_{RM}-like cells. A high abundance of tumor-infiltrating T_{RM}-like cells, quantified at tumor resection, has been associated with improved prognosis in multiple solid tumors,[19] including non-small cell lung cancer (NSCLC),[20,21] as well as with favorable responses to immune checkpoint blockade (ICB).[19] T_{RM}-like cells are cytotoxic[22] and secrete pro-inflammatory cytokines, such as IFNγ and TNF, that can recruit and influence the activation of tumor-specific T cells.[23,24] T_{RM}-like cells can also activate dendritic cells to increase the numbers of tumor-specific $CD8^+$ T cells, conferring protection to tumor cell re-challenge.[25] So-called "bystander" $CD8^+$ T_{RM}-like cells can therefore support the activity of tumor neoantigen-specific T cells.[26,27] How pre-existing T_{RM}-like cells within the healthy human lung may be impacted by cigarette smoking and whether these cells play a role in immune evasion by nascent tumors is unknown.

Avoiding destruction by the immune system is a hallmark of cancers.[28] "Immune evasion" refers to the loss of tumor immunogenicity under T cell predation.[29] The understanding of the mechanisms of immune escape have focused on tumor intrinsic factors, such as expression of ligands of immune checkpoint receptors (e.g., PD-L1), alterations in antigen presentation machinery, and neoantigen depletion.[30,31] Loss of heterozygosity (LOH) of the *HLA* locus and neoantigen depletion are observed in untreated NSCLC.[34,35] Neoantigen depletion is also enhanced after treatment with immune checkpoint inhibitors.[31] Tumor neoantigen evolution can therefore be defined as a system dependent on inputs (such as the degree of TMB and immune selective pressure) influenced by immune escape events to produce tumors with differing levels of immunogenicity.[32] Yet it is unclear whether the pre-cancerous immune environment in which a tumor develops influences the onset of immune evasion events and if this has implications for treatment with immunotherapy.

RESULTS

T_{RM}-like cell activity is enhanced in healthy lung tissue of ever-smokers

We first used flow and mass cytometry (CyTOF) to examine the proportion of $CD4^+$ and $CD8^+$ T cells with a T_{RM}-like phenotype (defined throughout as $CD3^+CD45RO^+CD45RA^-CCR7^-CD69^+CD103^{+/-}$) in the adjacent normal lung tissue from lung cancer patients undergoing surgical resection of tumors and from normal lung tissue obtained from deceased organ donors (Figure S1A and Tables S1, S2, S3, and S4). While the proportions of lung $CD4^+$ or $CD8^+$ T_{RM}-like cells did not change with individual age (37–83 years old; median 59 years old), sex, or cancer status, we observed a significant increase in the proportion of $CD8^+$ T_{RM}-like cells in the lung tissue of ESs compared with NSs (Figures 1A, 1B, S1B, and S1C). Within ES lungs, the increase in $CD8^+$ T_{RM}-like cells was not associated with the degree of smoking history (Figure S1D). Except for an increase in B cell proportion in ES lungs, we did not observe significant differences in any other major immune cell populations between ES and NS lungs (Figure S2). We next assessed the expression of T cell accessory molecules by T_{RM}-like cells to infer T cell activation state using validated CyTOF antibodies (Figure S3A). In the early phase of T cell activation, expression of co-stimulatory molecules such as CD28, CD27, 41BB, and OX40 predominates. At the peak of the T cell response, both co-stimulatory and co-inhibitory molecules are upregulated followed by a preponderance of co-inhibitory receptors (CD57, PD-1, LAG3, TIM3) toward the end of the response.[33] Global analysis of the expression of accessory molecules in lung-resident T cells revealed enhanced expression of CD27, CTLA-4, and ICOS in $CD4^+$ T_{RM}-like cells in ES patients, but not in resident T_{reg} or $CD8^+$ T_{RM}-like cells (Figures 1C, 1D, and S3B–S3D), translating to an

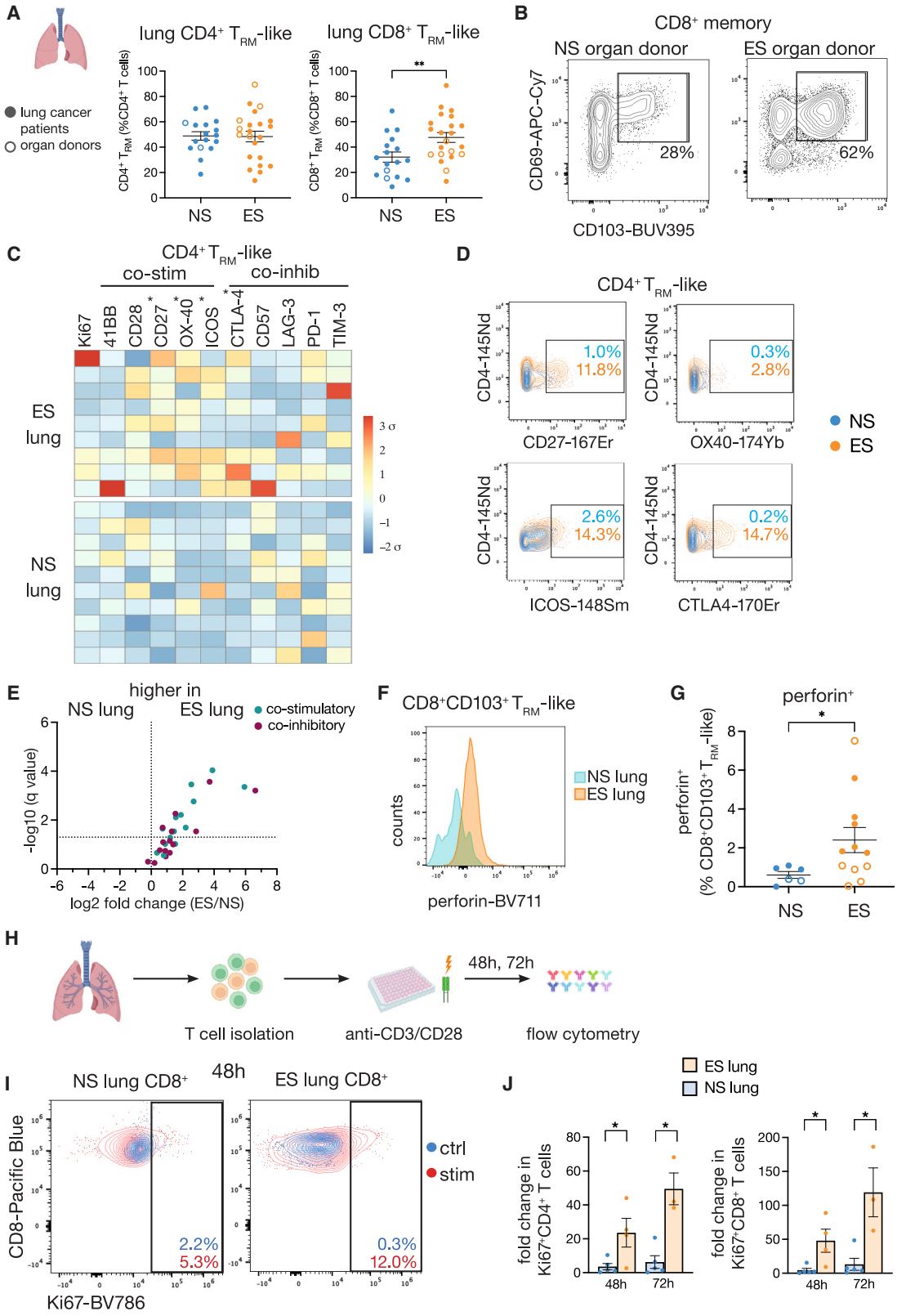

Figure 1. Lung resident memory-like T cells are less activated in never-smoker lung tissue

(A) Proportion of CD4+ T_{RM}-like and CD8+ T_{RM}-like cells in non-malignant lung tissue of lung cancer patients (filled circles) and healthy lungs of deceased organ donors (open circle) analyzed by CyTOF and flow cytometry. n = 17 NSs, n = 22 ESs. Data show mean ± SEM. Unpaired t test, *p < 0.05, **p < 0.01.

(legend continued on next page)

elevated overall abundance of co-stimulatory and co-inhibitory molecules in T_{RM}-like cells in the lungs of ESs (Figure 1E). Accordingly, a higher proportion of $CD8^+$ T_{RM}-like cells in ES lung tissue also expressed the effector molecule perforin compared with NS $CD8^+$ T_{RM}-like cells, indicating increased cytotoxic potential of these cells (Figures 1F and 1G). To further evaluate the activation status of T cells in ES and NS lungs, T cells were sort-purified from lung tissue, stimulated with anti-CD3/CD28, and proliferation was assessed 48 and 72 h later (Figure 1H). $CD4^+$ and $CD8^+$ T cells isolated from ES lung displayed heightened proliferation compared with NS $CD4^+$ and $CD8^+$ T cells (Figures 1I, 1J, and S3E). Taken together, these data provide evidence that T_{RM}-like cell activation is enhanced in ES lungs, and more generally, T cells within ES lungs are poised for effector function.

Early T_{RM}-like cell activation in ES tumors compared with NS tumors

The reduced activation status of T_{RM}-like cells from NS lungs led us to assess their phenotype throughout tumor evolution. Due to the difficulty of obtaining longitudinal tissue sampling of lung cancer patients, we use the multi-step progression of epithelial neoplasias from early-stage to late-stage cancer as a surrogate for time. We analyzed surgically resected primary lung tumors (stage I-IIIa, limited nodal metastases N0-2, M0) and biopsies of advanced primary tumors (stage IIIb-IV, extensive nodal metastases N2-N3, M0-1, Table S1) by CyTOF (Figure S4A and Table S4). Resident Tregs were enriched in both ES and NS early-stage tumors compared with matched normal tissue, consistent with previous reports[34] (Figure S4B). We also observed a greater proportion of $CD8^+$ T_{RM}-like cells in NS early-stage tumors compared with normal tissue, which was unchanged in late-stage tumors (Figure S4B). Analysis of accessory molecule expression revealed that $CD4^+$ and $CD8^+$ T_{RM}-like cells in ES patients exhibited a gradient of increased activation from non-malignant tissue to early-stage then to late-stage cancers (Figure 2A). However, T_{RM}-like cells within NS patients only showed evidence of activation in late-stage disease (Figure 2A). Indeed, comparing T_{RM}-like cell phenotypes between early-stage tumors from ES and NS patients demonstrated marked upregulation of accessory molecules in the former (Figure 2B), with key inhibitory molecules suggesting engagement of an exhausted phenotype in T_{RM}-like cells only in ES tumors (Figures S4C and S4D). Yet in late-stage cancers, this smoking-associated difference was abrogated (Figure 2C).

ESs may have heightened T_{RM}-like activity due to higher rate of respiratory infections. We therefore interrogated whether T_{RM}-like cells in ESs were tumor-specific by assaying the expression of CD39, a cell surface protein that distinguishes tumor-responsive from bystander T cells.[26,27] While there was an enrichment of tumor-responsive $CD39^+$ T_{RM}-like cells in tumors, there was no difference in their proportion according to smoking status in early-stage tumors (Figures 2D and 2E), suggesting polyclonal T_{RM}-like cell responses characterize ES and NS tumors. To determine whether the increase in T_{RM} cell activation in early-stage ES tumors was observed in a larger cohort of samples, we developed a $CD8^+$ T_{RM}-like cell transcriptional signature score from published bulk RNA-seq of $CD8^+$ T_{RM}-like cells isolated from NSCLC.[35] We then calculated the T_{RM}-like cell score in bulk RNA-seq data of early-stage LUAD from the TCGA cohort[7] and from the TRACERx cohort[36] that sampled multiple regions within a single tumor, including undifferentiated NSCLC that clusters with LUAD from principal component analysis, referred to as NSCLC-not otherwise specified (NSCLC-NOS; Figure S4E). Consistent with our CyTOF data, the $CD8^+$ T_{RM}-like cell score was lower in NS compared with ES early-stage tumors in both cohorts (Figure S4F). Within ESs, neither the $CD8^+$ T_{RM}-like cell score nor TMB was associated with levels of smoking exposure (Figure S4G). Linear regression modeling demonstrated only TMB was significantly associated with $CD8^+$ T_{RM}-like cell score in tumors ($p < 0.0001$), when assessing patient age, sex, disease stage, smoking status, presence of genomic smoking signature, mutational driver, and TMB (Figures 2F and S4H–S4J). However, TMB is known to be lower in NS tumors[37] (Figures 2F and S4F). Therefore, we analyzed ES samples with TMB comparable to NS samples ($\sqrt{TMB} < 3$, reflecting the FDA-approved cutoff of 10 mutations/megabase to select TMB^{hi} solid tumors for ICB[35]), which revealed a significantly lower $CD8^+$ T_{RM}-like cell score in NSs (Figure 2G). Indeed, within TRACERx tumors that demonstrated a variation in TMB score between regions (differences of more than five mutations/Mb between samples), we found these patients (all ES

(B) Representative flow cytometry plots showing CD103 versus CD69 expression, gated on $CD8^+$ T_{EM} from healthy lung tissue from an organ donor. ES donor (D35, 60-year-old female ex-smoker) and NS donor (D11; 56-year-old male).

(C) Heatmap of co-stimulatory and co-inhibitory molecule expression on $CD4^+$ T_{RM}-like cells in non-malignant lung tissue from cancer patients analyzed by CyTOF. Each column represents the average expression of each marker in $CD4^+$ T_{RM}-like cells in each ES and NS patient, and data are scaled to mean expression ± standard deviation per marker (*Z* score). Data excluded if <50 $CD4^+$ T_{RM}-like cells. n = 9 ES and n = 10 NS patients. Unpaired t test, *$p < 0.05$. Color scale indicates the *Z* score scaled by column/marker.

(D) Representative CyTOF plots of accessory molecule expression upon $CD4^+$ T_{RM}-like cells isolated from adjacent normal lung tissue from an ES cancer patient (AH0205, 83-year-old male ex-smoker) and a NS cancer patient (AH0059, 79-year-old female).

(E) Volcano plot depicting differential accessory molecule expression upon $CD4^+$ T_{RM}-like cells, resident T_{reg}, and $CD8^+$ T_{RM}-like cells, showing the log2 fold change between ES and NS lung for each marker per cell type. Co-stimulatory molecules are indicated in blue, and co-inhibitory markers are in dark red. The dotted line indicates q value = 0.05.

(F) Representative flow cytometry histogram showing the expression of perforin in $CD8^+CD103^+$ T_{RM}-like cells in a NS and an ES lung.

(G) Quantification of the proportion of $perforin^+$ cells within $CD103^+CD8^+$ T_{RM}-like cells by flow cytometric analysis of non-malignant lung tissue of cancer patients (filled circle) and healthy lung of organ donors (open circles), n = 6 NSs, n = 12 ESs. Data show mean ± SEM. Unpaired t test, *$p < 0.05$.

(H) Schematic of stimulation assay in total T cells isolated from non-malignant lung tissue of lung cancer patients.

(I) Representative flow cytometry plots of CD8 versus Ki67 expression 48 h after anti-CD3/CD28 stimulation of $CD8^+$ T cells sort-purified from non-malignant lung tissue. ES patient (MH0067, 47-year-old female, ex-smoker) and NS patient (MH0044, 47-year-old male).

(J) Fold change in the proportion of $Ki67^+$ $CD4^+$ and $CD8^+$ T cells at 48 h and 72 h after anti-CD3/anti-CD28 stimulation of T cells sorted from non-malignant lung tissue of lung cancer patients. n = 4 ESs; n = 5 NSs; Data show mean ± SEM. Unpaired t test, *$p < 0.05$. See also Figures S1, S2, S3, Tables S1, S2, S3, and S4.

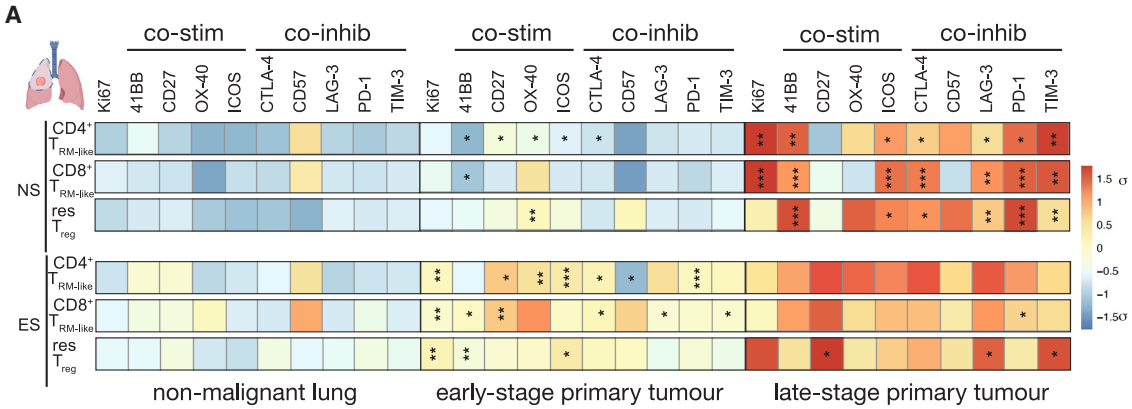

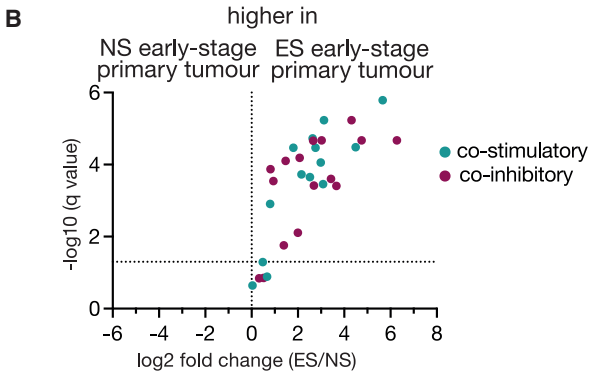

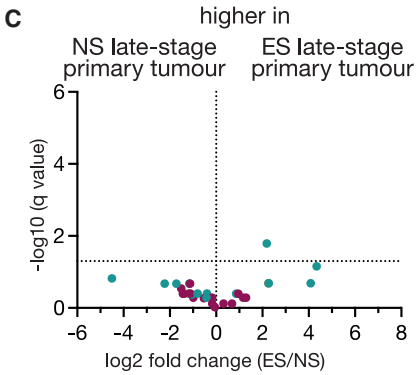

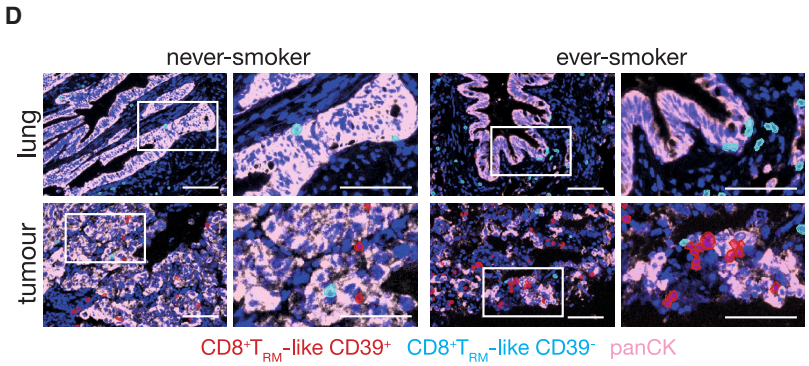

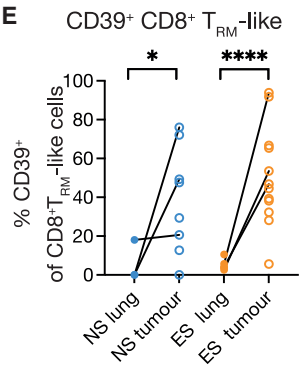

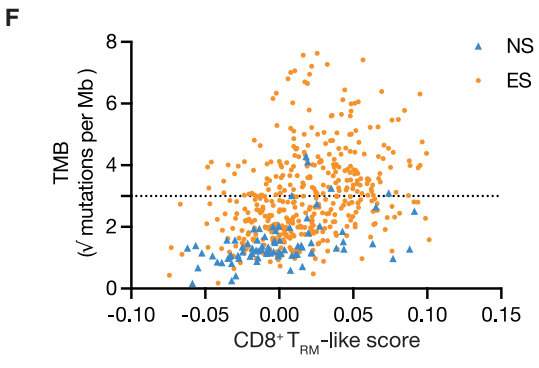

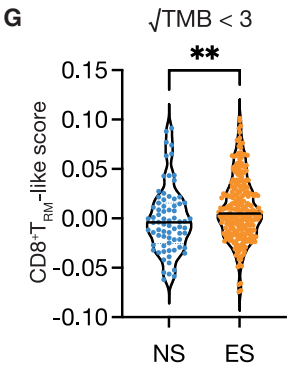

(legend on next page)

LUAD) had high T_{RM}-like cell scores (>0.01) regardless of TMB status (Figure S4K). These findings suggest that T_{RM} score may not be driven by TMB exclusively. More broadly, the collective data indicate that T_{RM}-like cell recruitment and activation likely occur earlier in ES lung tumorigenesis compared with NS patients.

T_{RM}-like cell induction prior to tumor onset enhances host immune cell recruitment and activation in a mouse model of lung adenocarcinoma

The increased frequency and heightened activation of T_{RM}-like cells within the normal lung tissue from ES individuals led us to model how pre-existing tumor-reactive or bystander lung T_{RM} cells might influence tumor-immune evolution, using mice orthotopically transplanted with lung cancer expressing the neoantigen ovalbumin (OVA) peptide (Figure 3A). Pre-existing, tumor-specific T_{RM}-like cells were generated by transferring effector $CD8^+$ OT-I TCR transgenic cells (congenically marked with CD45.1, referred to as donor cells) into C57BL/6 $CD45.2^+$ host mice that were treated intranasally (i.n.) with an inflammatory stimulus consisting of polyI:C and SIINFEKL-OVA peptide. This combination of local inflammation and antigen resulted in the generation of resident donor T_{RM}-like cells specifically in the lung as previously described[38] (Figures S5A and S5B; Table S5). The induction of host-derived OVA-specific $CD8^+$ T_{RM}-like cells detected with OVA-tetramer staining was minimal in this model (Figures S5C and S5D). Separately, we generated mice harboring lung T_{RM}-like cells of an irrelevant specificity by transferring $CD45.1^+$ $CD8^+$ gBT-I TCR transgenic cells (specific for herpes simplex virus glycoprotein B) into mice treated i.n. with poly:IC and gB peptide. Two weeks after T cell transfer and i.n. challenge, we could detect populations of non-circulating $CD45.1^+$ OT-I T_{RM}-like cells (tumor-specific: t-T_{RM} cells) and $CD45.1^+$ gBT-I T_{RM}-like cells (bystander: by-T_{RM}) (Figure 3B) with negligible induction of $CD45.2^+$ host $CD8^+$ T_{RM}-like cells (Figures S5C and S5E), demonstrating the efficacy and specificity of the model. A smaller population of T_{RM}-like cells was also detected in the lungs of mice injected with $CD45.1^+$ TCR transgenic cells in the absence of poly:IC and antigen stimulation; hence those groups were termed "lo t-T_{RM}" and "lo by-T_{RM}" mice (Figures 3A and 3B).

We then intravenously injected syngeneic $Kras^{G12D};p53^{\Delta/\Delta}$ lung cancer cells engineered to express the SIINFEKL-OVA peptide[39] (Figure S6A) to generate orthotopic lung tumors. Tumors were analyzed 8 weeks after tumor cell injection. The presence of pre-existing T_{RM}-like cells had no impact on tumor burden, although some mice in the no and low T_{RM} groups did not survive to day 70 and were collected for histological analyses only (Figures S6B–S6D). As expected, tumor-specific T_{RM}-like cell groups harbored higher proportions of donor $CD8^+$ T_{RM}-like cells expressing PD-1 at endpoint (day 70) compared with bystander T_{RM}-like group, indicating that the OVA^+ tumor cells supported enhanced expansion or retention of cognate donor T_{RM}-like cells (Figures S6E and S6F). We then investigated more broadly how T_{RM}-like cells present before tumor onset could affect the immune microenvironment. We found that high levels of pre-existing tumor-specific or bystander T_{RM}-like cells reshaped the host adaptive immune cell landscape within the tumor (Figure 3C). Greater proportions of host $CD8^+$ and $CD4^+$ T_{RM}-like cells developed in the high T_{RM}-like cell groups compared with low or no T_{RM} controls (Figures 3D and S6G). In turn, total host $CD8^+$ and $CD4^+$ $T_{em/eff}$ (includes T_{RM}) had greater PD-1 expression in the high T_{RM}-like cell groups (Figures 3E, 3F, and S6H), which was not observed in the spleen (Figure S6I). These data suggest that pre-existing tumor-reactive or bystander T_{RM}-like cells enhanced the activity of host T cells that were either newly recruited to the tumor microenvironment or primed by the initial inflammatory/antigen stimulation and expanded in the tumor. Dual staining of Ki67 and CD8 cells within tumors showed higher numbers of proliferating $CD8^+$ T cells in the high T_{RM}-like cell groups, confirming the flow cytometry data (green arrows, Figures 3G and 3H). Indeed, linear regression analysis revealed a strong positive correlation between the number of donor T_{RM}-like cells at endpoint with overall lung T cell number, whether the donor cells were tumor specific or bystander (Figure 3I). The number of Treg cells did not change between groups, although the percentage of $PD\text{-}1^+$ Treg cells was increased in the high T_{RM}-like cell groups (Figures 3C, S6J, and S6K). Overall, these data demonstrate that pre-existing T_{RM}-like cells in lung tissue, irrespective of TCR specificity, enhance T cell recruitment and activation in the resulting tumor microenvironment.

Figure 2. Tumor-associated T_{RM}-like cells have limited activation in early-stage never-smoker lung cancer

(A) Heatmap of co-stimulatory and co-inhibitory protein expression on $CD4^+$ T_{RM}-like cells, $CD8^+$ T_{RM}-like cells, and resident Treg cells isolated from lung tissue, stage I-IIIa (early-stage, surgically resected) primary tumors, and stage IIIb-IV (late-stage, metastatic) primary tumors as detected by CyTOF. Each column represents the average expression of each marker in ES and NS patients, and data are scaled to mean expression ± standard deviation per marker (Z score). n = 10 ES non-malignant lung, n = 10 ES early-stage tumors; n = 6 ES late-stage tumors; n = 10 NS non-malignant lung, n = 8 NS early-stage tumors; n = 5 NS late-stage tumors. Paired t test between matched patient lung and early-stage tumor tissue; unpaired t test between early-stage and late-stage tumors. *p < 0.05, **p < 0.01, ***p < 0.001. Statistical comparison between ESs and NSs not shown. Color scale indicates the Z score scaled by column/marker.

(B and C) Volcano plot depicting differential accessory molecule expression upon $CD4^+$ T_{RM}-like cells, resident T_{reg}, and $CD8^+$ T_{RM}-like cells, showing the average log2 fold change between (B) ES and NS early-stage tumor or (C) ES and NS late-stage tumor for each marker per cell type. Co-stimulatory molecules are indicated in blue, and co-inhibitory markers are in dark red. The dotted line indicates q value = 0.05.

(D) Representative images of ES and NS lung and corresponding tumors showing the expression of CD39 in $CD8^+$ T_{RM}-like cells. Red-rendered cells show $CD39^+CD8^+$ T_{RM}-like cells, and blue-rendered cells show $CD39^-CD8^+$ T_{RM}-like cells. Epithelial cells are stained with pan-cytokeratin (panCK, pink). Scale bar represents 50 μm.

(E) Quantification of the proportion of $CD39^+$ $CD8^+$ T_{RM}-like cells in NS and ES non-malignant lung and tumors. n = 3 NS lung, 8 NS tumors, 4 ES lungs, 12 ES tumors. Welch's t test. *p < 0.05; ****p < 0.0001.

(F) Scatterplot showing T_{RM} cell signature score and √TMB in RNA-seq data from TRACERx and TCGA LUAD and NSCLC-not otherwise specified (NOS) samples. n = 443 ESs, n = 74 NSs.

(G) Violin plot depicting the $CD8^+$ T_{RM}-like cell signature score in NS and ES lung tumors from TCGA and TRACERx cohorts in patients with low TMB (√TMB <3). n = 269 ESs, n = 74 NSs. Wilcoxon rank-sum test. **p < 0.01. See also Figure S4 and Tables S1 and S4.

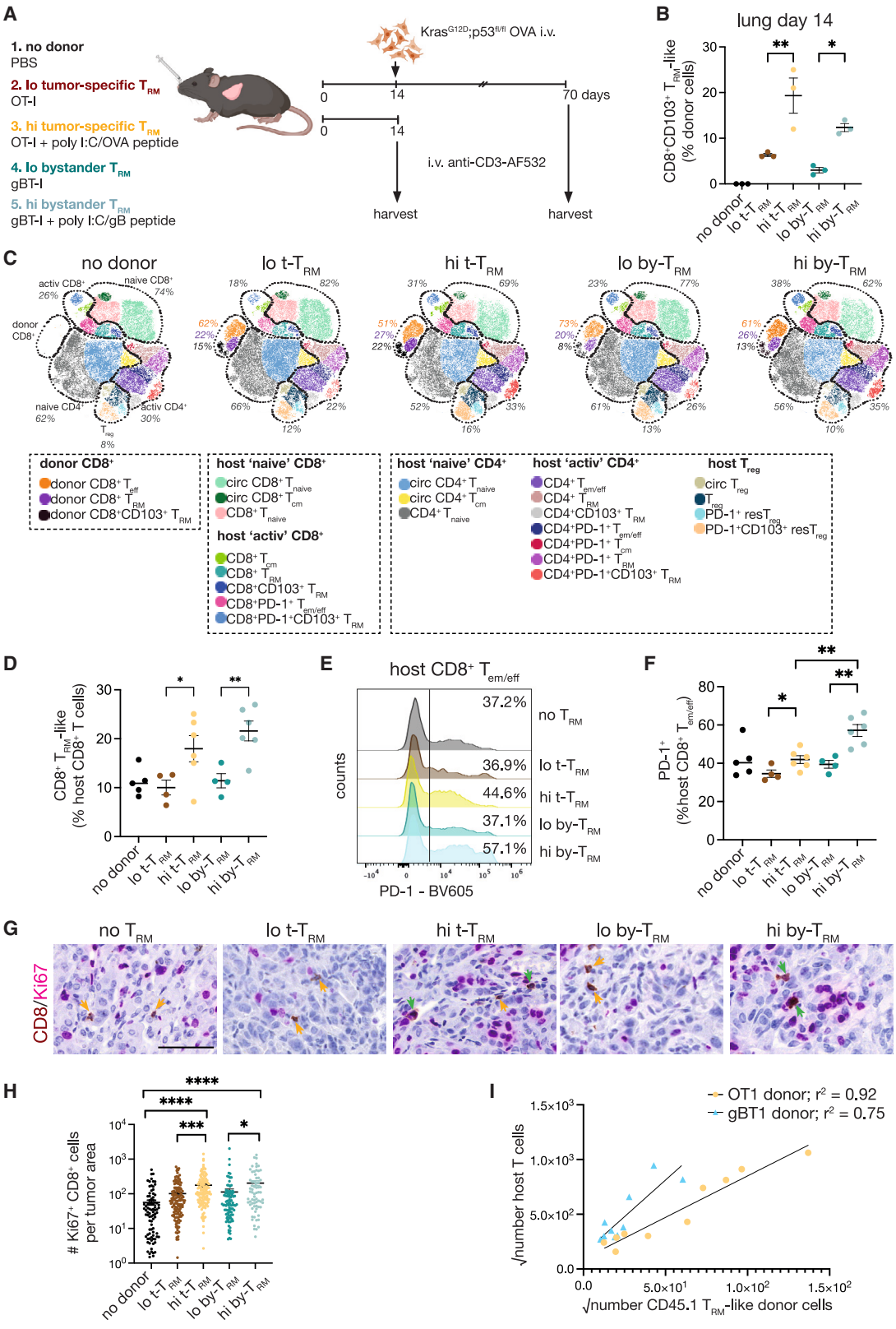

(legend on next page)

Pre-existing T_{RM}-like cells promote immune evasion events in lung adenocarcinoma *in vivo*, resulting in resistance to immune checkpoint blockade

Given the increased T cell activity observed in tumors grown in a T_{RM}-rich environment, we investigated whether this enhanced "immune pressure" could drive immune evasion by tumor cells. Although high levels of pre-existing T_{RM}-like cells did not affect overall tumor burden (Figures S6B–S6D), we found that a greater proportion of tumors in these groups had lost presentation of the SIINFEKL-OVA neoantigen, a sign of immune escape (Figures 4A and 4B). Likewise, we observed substantial loss of total surface protein expression of H-2Kb, an MHC class I protein, on tumor cells in the high T_{RM}-like cell groups (Figures 4C and 4D, gating strategy in S7A and S7B), another known mechanism of immune escape. This loss of antigen presentation capacity was not associated with impaired IFNγ signaling: IFNγ expression was increased in $CD4^+$ and $CD8^+$ $T_{eff/em}$ from the hi-T_{RM} tumors (a further sign of increased activation) (Figures S7C–S7E), and phospho-STAT1 levels in tumor cells were unchanged among the different subgroups (Figures S7C and S7D). Antigen-presenting cells were rare, and the frequency of NK cells was similar in all groups, as well as in NS and ES patient tumors (Figures S7C, S7D, S7F, and S7G). Overall, these data indicate that the presence of lung T_{RM}-like cells of any specificity prior to tumor formation enhances immune escape mechanisms in tumor cells, even in an environment rich in IFNγ. To determine the therapeutic implications of these findings, we evaluated the response to combination anti-PD-1 and anti-CTLA-4, a combination immunotherapy that was found to improve survival in advanced NSCLC patients (>1% tumor PD-L1 expression) compared with anti-PD-1 monotherapy in a descriptive analysis.[40] The polyI:C/OVA and low T_{RM} control groups showed partial responses to combination ICB, withstanding tumor growth a further 20 and 12 days (median survival of 64 and 56 days respectively, Figure 4E) compared with control IgG-treated groups. However, tumors that arose in a T_{RM}-like rich environment (hi t-T_{RM}) were completely resistant to combination ICB (median survival of 44 days, Figure 4E). Together these results show that in this model, pre-existing T_{RM}-like cells accelerate the onset of immune escape mechanisms in tumor cells, resulting in reduced response to checkpoint immunotherapy.

Early immune escape events are only detected in ES tumors

These results prompted us to evaluate whether tumor-immune evolution might be impacted differentially in ES and NS tumors given that they arise in microenvironments with distinct T_{RM}-like cell activity. Recent studies have defined a system of tumor evolution as one dependent upon inputs, including TMB and the level of immune selective pressure, that influence immune escape events such as loss of heterozygosity of *HLA-A*, *-B*, or *-C* alleles (*HLA* LOH) and non-synonymous mutations in genes encoding for antigen presentation machinery elements (APM).[32] Given the substantial differences in TMB and "immune pressure" identified with smoking status, lung cancer occurring in ES and NS patients provides an opportunity to define the evolution of tumor immune escape using real-world data. To infer the timing of immune escape events such as *HLA* LOH and mutations in APM genes (APM^{mut}, using published gene lists[32]), we used multi-site sequencing data to distinguish early escape events detected in all sites (clonal events) from events occurring later in evolution, detected in only one or some sites (subclonal events). We analyzed *HLA* LOH and APM^{mut} in four separate cohorts of pre-invasive LUAD, early-stage LUAD, and late-stage lung cancer (Figure 5A and Table S4)[36,41,42,43]. We first used the well-annotated TRACERx cohort to explore both cell-intrinsic and -extrinsic determinants of *HLA* LOH. Although we observed the overall occurrence of clonal or subclonal *HLA*

Figure 3. T_{RM}-like cells present in the lung before tumor onset increase the recruitment and activation of host T cells in lung adenocarcinomas, irrespective of their tumor specificity

(A) Schematic of the experimental design. CD45.1 donor T cells specific to OVA (OT-I) or gB (gBT-I) were adoptively transferred into CD45.2 hosts with and without intranasal co-administration of polyI:C and OVA or gB peptides to generate high and low levels of $CD8^+T_{RM}$ -like cells specific to OVA ($CD45.1^+$ tumor-specific OT-I T_{RM}-like cells: t-T_{RM} cells) or gB ($CD45.1^+$ bystander gBT-I T_{RM}-like cells: by-T_{RM}) compared with no T_{RM} controls. Lung tumor cells generated from a $Kras^{G12D/+};p53^{flox/flox}$ mouse were engineered to express OVA (KP-OVA) and injected 2 weeks after transfer of CD45.1 cells to generate experimental groups with pre-existing T_{RM}-like cells specific to the tumor OVA antigen (t-T_{RM}) or pre-existing T_{RM}-like cells reactive to gB (by-T_{RM}). Lungs were collected either prior to tumor cell injection (n = 3/group) or 8 weeks after tumor cell injection (n = 6/group). Mice were injected with anti-CD3-AF532 5 min before collection to label circulating T cells.

(B) Quantification of $CD8^+CD103^+$ T_{RM}-like donor cells in the lungs of recipient mice 2 weeks after T cell transfer and prior to KP-OVA tumor cell injection by flow cytometry. n = 3 mice/group. Data show mean ± SEM. Unpaired t test, $^*p < 0.05$, $^{**}p < 0.01$.

(C) Representative tSNE plots generated from flow cytometry data of 40,000 host and donor T cells from tumor-bearing lungs collected at day 70. Plots depict combined data from four mice per group with comparable tumor burdens. Percentages of donor T cell types calculated as proportion of donor $CD8^+$ T cells; percentages of host $CD4^+$ "naïve" (circulating and naive host cells), "activ" (effector and resident host cells), and T_{reg} cells calculated as a proportion of host $CD4^+$ T cells; percentages of "naïve" and "activ" $CD8^+$ T cells calculated as a proportion of host $CD8^+$ T cells. As donor T cells differ between groups, proportions as shown allow for ease of comparison between experimental groups.

(D) Proportion of host $CD8^+$ T_{RM}-like cells in the lungs of mice collected at day 70 determined by flow cytometry. n = 4–6 mice per group. Data show mean ± SEM. Unpaired t test, $^*p < 0.05$; $^{**}p < 0.01$.

(E) Representative histogram showing the expression of PD-1 in host $CD8^+$ $T_{eff/EM}$ cells in the lung of mice collected at day 70.

(F) Percentage of PD-1^+ cells among host $CD8^+$ $T_{eff/EM}$ cells in the lung of mice collected at day 70. n = 4–6 mice per group. Data show mean ± SEM. Unpaired t test, $^*p < 0.05$; $^{**}p < 0.01$.

(G) Representative images showing the expression of CD8 (brown) and Ki67 (purple) in lung tumors in the indicated groups determined by dual immunohistochemistry. Scale bar represents 100 μm. Yellow arrows: $CD8^+$ cells, green arrows: $Ki67^+CD8^+$ cells.

(H) Quantification of the number of $CD8^+Ki67^+$ cells in individual lung tumors relative to each tumor area (mm^2). Data are mean ± SEM. n = 6 mice per group. Unpaired t test, $^*p < 0.05$; $^{***}p < 0.001$, $^{****}p < 0.0001$.

(I) Linear regression analysis of the number of total host $CD3^+$ T cells with the number of donor $CD8^+$ T_{RM}-like cells in the lung of mice from tumor-specific $CD8^+T_{RM}$-like group (yellow) and the bystander $CD8^+T_{RM}$-like group (blue), analyzed at day 70. See also Figures S5, S6, and Table S5.

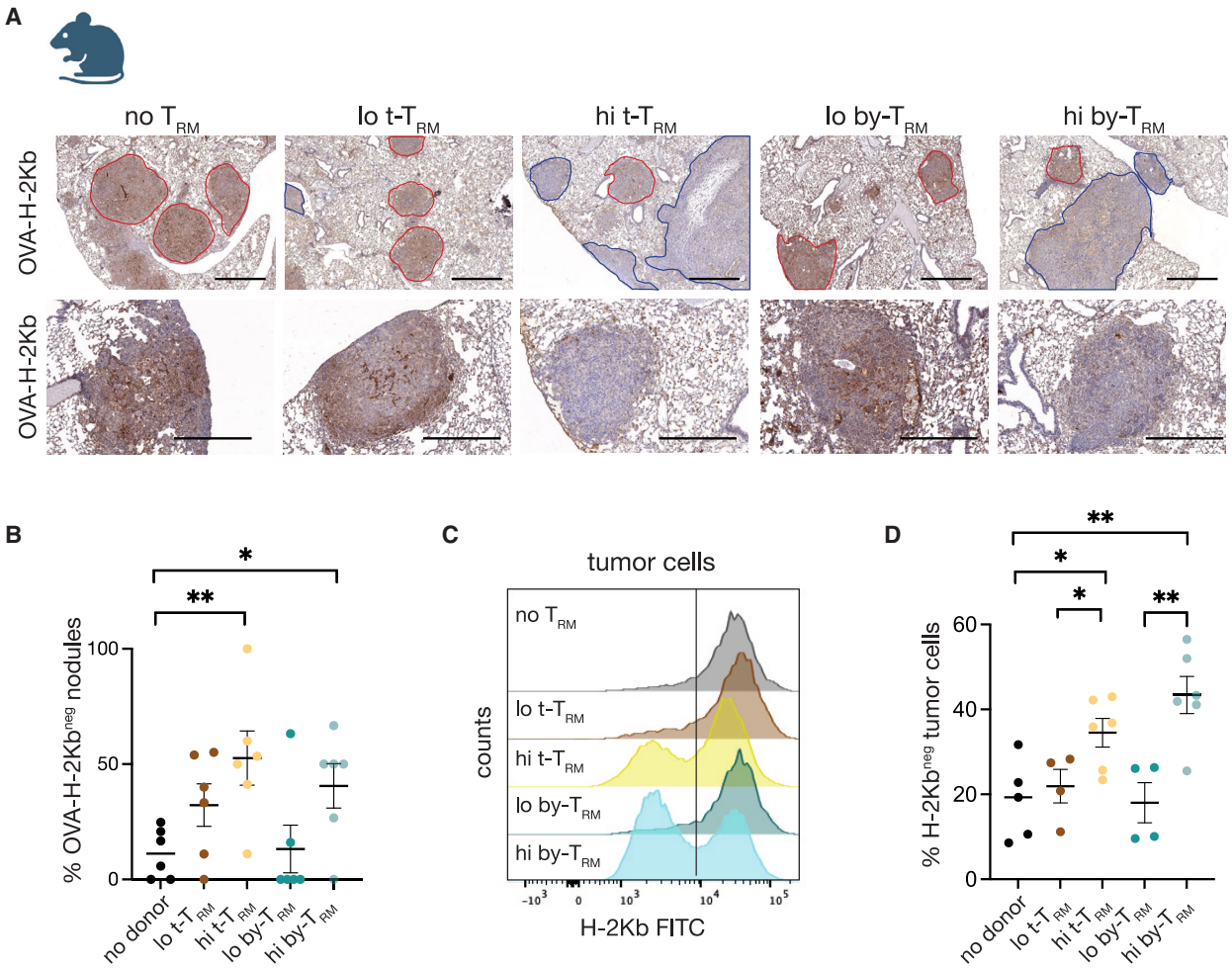

(legend on next page)

LOH or *APM*^{mut} was associated with TMB, these immune escape events were also observed in some tumors with low TMB (Figure 5B). *HLA* LOH or *APM*^{mut} was not associated with immune infiltrate,[35] clonal driver mutation status, and genomic smoking signature (Figures S8A and S8B), suggesting immune escape by *HLA* LOH is not linked to these features, which were determined at the time of tumor collection. Critically, clonal *HLA* LOH or *APM*^{mut} events were never observed in NS tumors (Figure 5C). Indeed, in all multi-site cohorts analyzed, clonal *HLA* LOH or *APM*^{mut} was only ever detected in ES tumors (Figure 5D, Fisher's exact test, two-tailed p = 0.001 and p = 0.002, respectively). Subclonal events were also more frequent in ES tumors, indicating a higher rate of immune evasion events in ES tumors in general. The observation that genomic smoking signature was not associated with immune escape events (Figures S8A and S8B), but that smoking history was (Figure 5D), further demonstrates the influence of an inflamed immune microenvironment, here induced by smoking, in driving tumor immunogenicity, in addition to tobacco-induced mutagenesis. Multi-site data were not available for pre-invasive lesions to determine the clonality of LOH, yet 2/20 ES lesions had *HLA* LOH compared with 1/62 NS lesions (Figure 5E). Combining all datasets representing multiple stages of lung cancer progression, *HLA* LOH was a rare event in NS tumors (Figure S8C, Fisher's exact test, two-tailed $p < 10^{-8}$) and occurred mostly in ES tumors, indicating immune escape is a continuous event in ES tumors that likely starts early in their evolution.

Overall, these data, combined with data from our LUAD mouse model, suggest that immune escape is related to the environment in which the tumors arise and imply that the timing of "immune pressure" is an important determinant of tumor immunogenicity, in addition to levels of immune infiltration and TMB.

DISCUSSION

Adaptive immunity influences multiple stages of tumor evolution. Cancer immunosurveillance involves elimination of early malignant cells following T cell recognition of neoantigens. Later, pre-malignant cells that escape elimination can form pre-invasive lesions held in check by cancer-immune equilibrium. Finally, immune escape involves the development of tumor mechanisms to evade immune predation, enabling invasive lesions to form.[2,44] T_{RM} cells have been shown to be involved in cancer-immune equilibrium,[3] and their abundance in resected invasive cancers correlates with better outcomes.[19] Yet, it has been unclear the extent to which pre-existing T_{RM}-like cells influenced by environmental insults may shape the immunogenic evolution of tumors.

Our deep profiling of immune cells in healthy lung and early-stage and late-stage primary tumors provides a surrogate for the longitudinal analysis of resident T cells in states of pre-malignancy, early tumor formation, and progression. We observed that chronic cigarette smoking correlated with enhanced T_{RM}-like cell immunosurveillance in human lungs. This heightened immune pressure selected for tumor clones capable of immune evasion. In a murine model, we found that both tumor-specific and bystander $CD8^+$ T_{RM}-like cells increased the activity and recruitment of T cells to the tumor, initiating early loss of MHC class I. These data identify a critical additional "input" to the system of tumor evolution[32]—the timing of immune pressure—which acts as an additional regulator of tumor "visibility" to the immune system.

$CD8^+$ T_{RM}-like cells in the skin have been shown to protect against melanoma formation, promoting cancer-immune equilibrium.[3] Patients with vitiligo, an autoimmune skin condition characterized by high T_{RM}-like cell infiltration, have a lower prevalence of malignant melanoma.[45,46] Further studies in mice demonstrated immune predation by T_{RM}-like cells is critical in vitiligo-associated cancer protection, indicating that resident T cell memory is a likely key element in the prevention of tumor onset in the skin.[47] Our discovery of T_{RM}-like cell immunosurveillance in ES lungs provides insight into tumor formation in both NS and ES patients. Oncogenic alterations and genomic instability are found in normal lung basal cells from heavy smokers,[4,5] yet not all develop lung cancers.[48] Pre-invasive LUSC[49] possess mutations in oncogenic drivers including *KRAS*, *EGFR*, and *KEAP1*, but a number of these lesions regress to a normal-like state.[50] Infiltration of $CD8^+$ and $CD4^+$ T cells has been described in pre-malignant LUSC and LUAD lesions[51,52] and proposed to support the elimination of malignant cells.[50] It is tempting to speculate greater T_{RM}-like cell immunosurveillance associated with tobacco smoking may protect from invasive cancers induced by this same insult. Future studies evaluating the degree of T_{RM}-like cell immunosurveillance within ES and NS pre-invasive LUAD would shed light on this question. A limitation of our study is the analysis of independent cohorts that represent a surrogate for longitudinal analysis of tumor evolution. Nevertheless, our work suggests that the timing of immune recognition of tumors, as influenced by the pre-existing immune landscape in the organ of origin, is a critical regulator of tumor evolution.

Once the cancer-immune equilibrium is broken and tumors are established, high abundance of T_{RM}-like cells in tumors has been associated with better patient outcome in multiple solid

Figure 4. Lung T_{RM}-like cells existing before tumor onset initiate immune escape mechanisms in a mouse model of lung adenocarcinoma, reducing sensitivity to immune checkpoint inhibitors

(A) Representative images showing the presentation of OVA-H-2Kb complexes by lung tumors in the indicated groups. Tumors contoured in red are OVA-H-2Kb positive, tumors contoured in blue are OVA-H-2Kb negative. Scale bar top panel represents 1 mm, and bottom panel bar represents 500 μm.

(B) Percentage of OVA-H-2Kb-negative tumor nodules from immunohistochemistry staining. n = 6 mice/group. Data are mean ± SEM. Unpaired t test, $^{**}p < 0.01$, $^{*}p < 0.05$.

(C) Representative histogram showing the surface expression of H-2Kb by tumor cells in the lung of mice collected at day 70.

(D) Percentage of H-2Kb-negative tumor cells measured by flow cytometry. n = 4–6 mice/group. Data are mean ± SEM. Unpaired t test, $^{**}p < 0.01$, $^{*}p < 0.05$.

(E) Kaplan-Meier survival curve showing the survival of mice after injection of KP-OVA cells in hi-t-T_{RM} (polyI:C/OVA i.n + OT-I donor cells i.v.), lo t-T_{RM} (PBS i.n + OT-I donor cells i.v.), and polyI:C/OVA control (polyI:C/OVA i.n. + PBS i.v.) mice and treated with anti-PD-1 + anti-CTLA-4 or rat IgG2a + hamster IgG controls. Log rank Mantel Cox test of anti-PD-1 + anti-CTLA-4-treated mice comparing hi t-T_{RM} mice with lo t-T_{RM} and polyI:C/OVA control mice, $^{**}p < 0.01$. n = 6 mice/group. See also Figure S7.

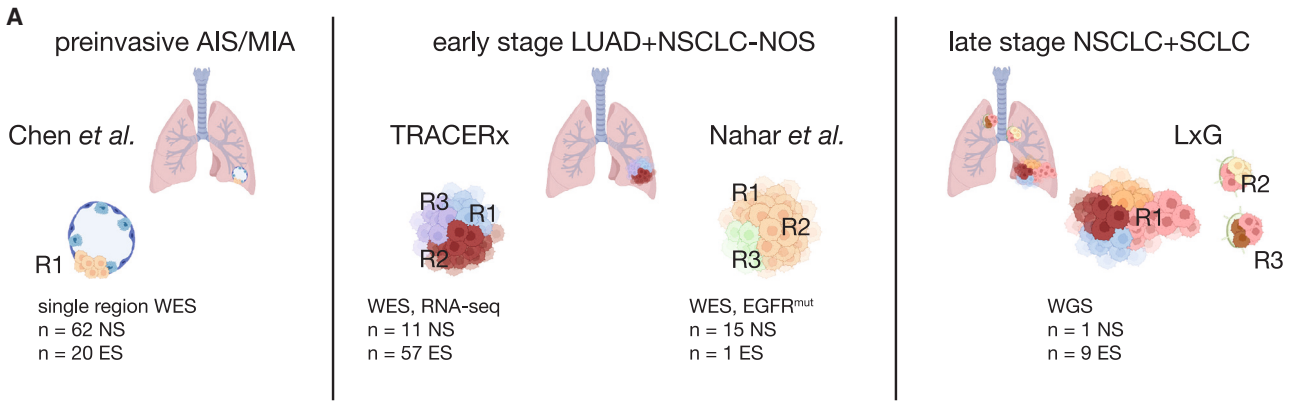

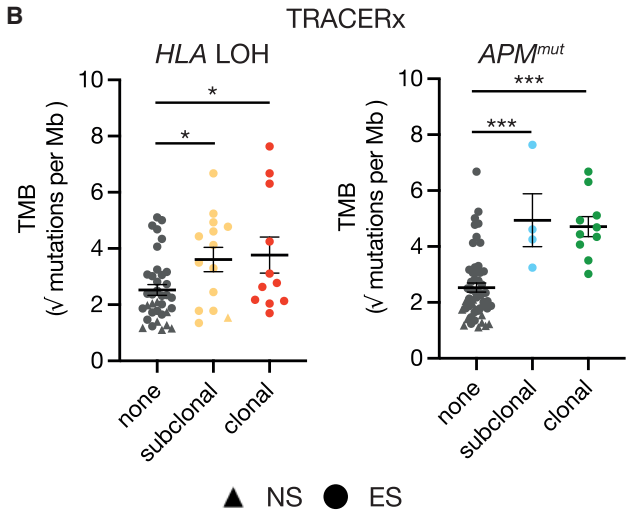

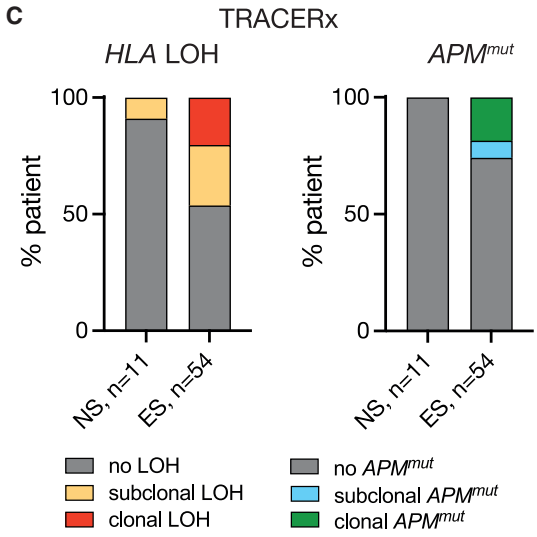

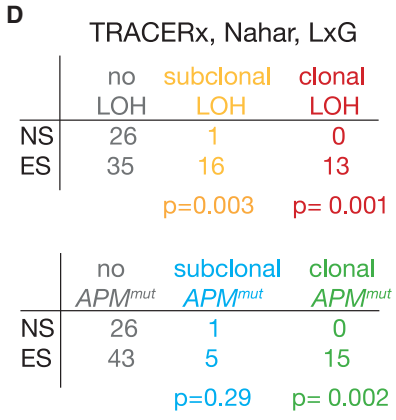

	no LOH	subclonal LOH	clonal LOH
NS	26	1	0
ES	35	16	13
		p=0.003	p= 0.001

	no APM^{mut}	subclonal APM^{mut}	clonal APM^{mut}
NS	26	1	0
ES	43	5	15
		p=0.29	p= 0.002

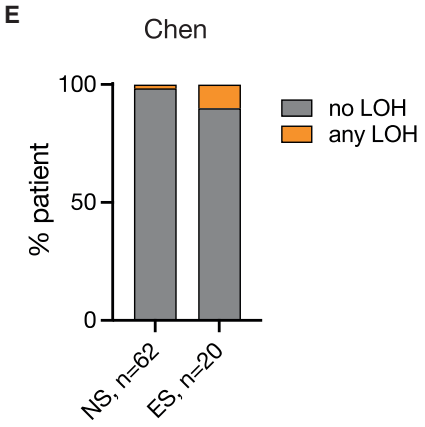

Figure 5. Early immune escape events are only detected in ES tumors

(A) Schematic of the four patient cohorts in which *HLA* LOH was evaluated, and multi-site data allowed the detection of subclonal or clonal *HLA* LOH. AIS, adenocarcinoma *in situ*; MIA, minimally invasive adenocarcinoma; LUAD, lung adenocarcinoma; NSCLC-NOS, non-small cell lung cancer not otherwise specified; SCLC, small cell lung cancer; WES, whole-exome sequencing; WGS, whole-genome sequencing; R, region.

(B) Dot plot showing TMB in TRACERx LUAD and NSCLC-NOS tumors separated according to the presence of early immune escape (clonal *HLA* LOH or APM^{mut}), late immune escape (subclonal *HLA* LOH or APM^{mut}), or absence of *HLA* LOH (gray). NSs are depicted in triangles and ESs in circles. n = 41 patients. One way ANOVA, *p < 0.05; **p < 0.01; ***p < 0.001. Data are mean ± SEM.

(C) Proportion of patients with clonal or subclonal *HLA* LOH or APM^{mut} according to smoking history in early-stage TRACERx LUAD + NSCLC-NOS tumors (Fisher's exact test, p = 0.06 for *HLA* LOH, p = 0.11 for APM^{mut}).

(legend continued on next page)

tumors including breast cancer,[53] melanoma,[25] and NSCLC.[18,19] Correlative studies in NSCLC, melanoma, breast, and oral cancer have reported an association between tumor infiltration of $CD8^+$ T cells with a residency phenotype and response to ICB.[35,54–56] In contrast, here we explored how T_{RM}-like cells existing in the lung before tumor onset regulated immune escape. In this context, the T_{RM}-like cell infiltrate at the time of collection may not accurately reflect the environment in which the tumor initially arose. Instead, we find that smoking history is a better indicator of the environment in which the tumor grew, with ES lungs having a higher abundance and activation of T_{RM}-like cells than NS lungs. The direct comparison of tumor evolution of cancers that arose in lungs with a low or high T_{RM}-like cell environment as observed in human ES and NS lungs and an experimental mouse model enabled to reveal how tumor growth in a T_{RM}-like cell-rich milieu impacts tumor evolution.

Selective pressure applied by the immune system promotes immune evasion mechanisms in tumor cells and has implications for treatment of patients with ICB. One such escape mechanism involves silencing of the APM,[54] including loss of MHC class I by genetic, epigenetic, or post-translational modifications or mutations in the antigen presentation pathway. Consistent with previous work,[55,56] we observed that *HLA* LOH occurred in tumors of low and high mutational load. Strikingly, clonal *HLA* LOH and APM^{mut} were only detected in ES patients, suggesting they are an early event in the evolution of ES tumors. Analysis of *HLA* LOH in pre-invasive lung cancer lesions corroborates this observation where *HLA* LOH occurred in 34% of squamous carcinoma *in situ* in ES patients,[50] 10% of adenocarcinoma *in situ*/minimally invasive adenocarcinoma in ES patients, and only 1% of these lesions in NS patients.[41] Our finding that elevated T_{RM}-like cells and T cell activation are features of the ES lung is consistent with their capacity to exert early immune pressure in this context. Analysis of expanded TCR clones in tumor multi-region sequencing of ES tumors showed that $CD8^+CD103^+$ T_{RM}-like cells were composed of a high proportion of ubiquitous TCR clones (present in all tumor regions), indicative of early recruitment of these T_{RM}-like cells to the tumor site. In contrast, regional TCR clones, present only in some tumor regions, were poorly represented in T_{RM}-like cells.[57] These results concur with our finding that T_{RM}-like cells are key components of the early immune microenvironment in ES LUAD and orchestrate immune cell recruitment. Indeed, our data from preclinical models directly demonstrate that high T_{RM}-like cell abundance, irrespective of TCR specificity, is sufficient to orchestrate a microenvironment that impels early immune escape events in cancer. Therefore, we propose that the T_{RM}-like rich microenvironment of ES lungs where NSCLC grows is a likely driver of this early immune evasion mechanism.

Importantly, *HLA* LOH is a strong predictor of poor response to ICB in LUAD.[55] Although ESs with NSCLC are thought to be best responders to ICB, only a small proportion of patients respond to therapy.[58] Our work provides insight into the diversity of responses observed within this group. Our data using a $Kras^{G12D};p53^{\Delta/\Delta}$ mouse model of LUAD showed that the loss of MHC class I induced by an activated T_{RM}-like environment abolished sensitivity to ICB. We propose that ES tumors are under immune pressure from their inception, forcing early onset of immune escape mechanisms in a subset of patients, which ultimately leads to their insensitivity to ICB. In contrast, NS patients presented as a relatively homogeneous group whose tumors evolved in a dearth of immune selection pressure, resulting in less immune escape of tumor clones. However, low T cell activation and the relatively small numbers of neoantigens in these NS tumors diminish chances for T cell recognition, so generating a *de novo* anti-tumor response with blockade of co-inhibitory molecules has not proved successful for NS patients.[12] We propose ES tumors that arise in an active T_{RM}-like environment may benefit from combination immunotherapy aiming to activate antigen presentation. In contrast, tumors grown in T_{RM}-like poor environments, such as those occurring in NS, could paradoxically have favorable features for certain immune interventions due to the absence of early selective pressure for tumors to become immunologically silent. This lack of immune pressure increases the potential of tumor cell populations to be targeted *en masse* by T cell recognition of intact APM. Alternative immunotherapeutic approaches for NS patients may lie in the activation of co-stimulatory molecules, personalized neoantigen vaccines, or cell therapy with tumor-reactive T cells targeted to these clonal neoantigens.[59–62]

Our study indicates that T_{RM}-like cells immunosurveillance associated with cigarette smoking before the onset of malignancy exerts an early selective pressure that acts in addition to tumor cell-intrinsic characteristics to shape tumor evolution in lung cancer. T_{RM}-like cells present in other solid organs, such as the skin or the breast, might be similarly impacted by environmental insults or physiological dynamics throughout an organism's lifespan that in turn control cancer immunosurveillance and tumor evolution.

STAR★METHODS

Detailed methods are provided in the online version of this paper and include the following:

- KEY RESOURCES TABLE
- RESOURCE AVAILABILITY
  - Lead contact
  - Materials availability
  - Data and code availability
- EXPERIMENTAL MODEL AND SUBJECT DETAILS
  - Patient samples
  - $Kras^{G12D/+};p53^{flox/flox}$-OVA murine lung cancer cell line
  - Mice
- METHOD DETAILS
  - *In vivo* formation of T_{RM} and lung tumors
  - Quantification of tumor burden and multiplex immunostaining

(D) Fisher's exact test of combined multi-site data from the TRACERx, Nahar, and LxG cohorts depicting the number of patients with no, subclonal, or clonal *HLA* LOH events. Fisher's exact test comparing clonal or subclonal mutations to no mutation.
(E) Proportion of patients with clonal or subclonal *HLA* LOH according to smoking history in pre-invasive lesions (Chen cohort, Fisher's exact test, $p = 0.14$). See also Figure S8 and Table S4.

- Treatment study
- Mouse organ preparation for flow cytometry analysis
- Human lung and tumor cell preparation
- Mass cytometry
- Analysis of mass cytometry data
- Flow cytometry
- Human lung T cell *in vitro* assays
- Immunohistochemistry and multiplex immunostaining
- Patient datasets
- Tumor mutational burden
- T_{RM}-like cell signature score in RNA-seq data
- HLA typing and LOH calling

● QUANTIFICATION AND STATISTICAL ANALYSIS

SUPPLEMENTAL INFORMATION

Supplemental information can be found online at https://doi.org/10.1016/j.ccell.2023.03.019.

ACKNOWLEDGMENTS

We thank Dr. Alexandra Garnham for advice on analyzing CyTOF data, Dr. Alissa Robbins for T cell reagents and CyTOF advice, and Dr. Sarah Best for mouse model advice and critical reading of the manuscript. We thank WEHI facilities including Histology (Emma Pan and Ellen Tsui), Flow Cytometry (Simon Monard), and Bioservices (Shannon Oliver, Eren Loza, Keti Florides, Louise Spencer) for expert advice and performing experiments. The MR1 tetramer technology was developed jointly by Dr. James McCluskey, Dr. Jamie Rossjohn, and Dr. David Fairlie, and the material was produced by the NIH Tetramer Core Facility as permitted to be distributed by the University of Melbourne. We are grateful to the Victorian Cancer Biobank and all lung cancer patients who participated in this study. We gratefully acknowledge the generosity of the organ donor families in providing valuable tissue samples to the Australian Donation and Transplantation Biobank. This work was performed in part at the Materials Characterisation and Fabrication Plat-form (MCFP) at the University of Melbourne under Andrew Mitchell's leadership, and the Victorian Node of the Australian National Fabrication Facility (ANFF), with support from the Victorian Comprehensive Cancer Centre under the Resistance to Targeted Therapies Program. The mass cytometry studies were also supported in part by the Australian Cancer Research Foundation. C.E.W. is supported by a Lung foundation Australia/Deep Manchanda Early Career Fellowship and a Cure Cancer/Cancer Australia Priority-driven Collaborative Cancer Research grant (1163900). J.A.M. is supported by a University of Melbourne Research Scholarship. K.D.S. and C.E.T. are supported by a Victorian Cancer Agency Mid-Career Research Fellowship (20026 and 18003), and K.D.S. is supported by the Peter and Julie Alston Centenary Fellowship. C.L.G. is supported by funding from an NHMRC Early Career Fellowship (GNT1160963). D.H.D.G is supported by Australian NHMRC Fellowships/grants (1090236, 1158024 and 1145888), Cancer Council Victoria Grants-in-Aid (1146518 and 1102104). M.L.A.L. is supported by funding from the Viertel Foundation Senior Medical Research Fellowship. This work is supported by an NHMRC Ideas Grant (GNT1182155), The Harry Secomb Trust, the Jenny Tatchell Fund, and by funds from the Operational Infrastructure Support Program provided by the Victorian Government and NHMRC IRIISS (Independent Research Institutes Infrastructure Support Scheme) Grant. C.S. is a Royal Society Napier Research Professor (RSRP\R\210001). His work is supported by the Francis Crick Institute that receives its core funding from Cancer Research UK (CC2041), the UK Medical Research Council (CC2041), and the Wellcome Trust (CC2041). C.S. is funded by Cancer Research UK (TRACERx (C11496/A17786), PEACE (C416/A21999) and CRUK Cancer Immunotherapy Catalyst Network); Cancer Research UK Lung Cancer Centre of Excellence (C11496/A30025); the Rosetrees Trust, Butterfield and Stoneygate Trusts; NovoNordisk Foundation (ID16584); Royal Society Professorship Enhancement Award (RP/EA/180007); National Institute for Health Research (NIHR) University College London Hospitals Biomedical Research Centre; the Cancer Research UK-University College London Centre; Experimental Cancer Medicine Centre; the Breast Cancer Research Foundation (US) (BCRF-22-157); Cancer Research UK Early Detection and Diagnosis Primer Award (grant EDDPMA-Nov21/100034); and The Mark Foundation for Cancer Research Aspire Award (grant 21-029-ASP). This work was supported by a Stand Up To Cancer-LUNGevity-American Lung Association Lung Cancer Interception Dream Team Translational Research Grant (grant number: SU2C-AACR-DT23-17 to S.M. Dubinett and A.E. Spira). Stand Up To Cancer is a division of the Entertainment Industry Foundation. Research grants are administered by the American Association for Cancer Research, the Scientific Partner of SU2C. C.S. is in receipt of an ERC Advanced Grant (PROTEUS) from the European Research Council under the European Union's Horizon 2020 research and innovation programme (grant agreement no. 835297).

AUTHOR CONTRIBUTIONS

Conceptualization, C.E.W., D.H.D.G., M.-L.A.-L; methodology, C.E.W., L.K.M., C.E.T., D.H.D.G., M.-L.A.-L; formal analysis, V.G., K.Y., N.T.R., M.T., T.P.S.; investigation, C.E.W., C.M., D.B., T.T., A.C., S.C., C.E.T., A.J.M., L.C.R., A.O.; resources, J.A.M., K.D.S., V.J.S., G.S., R.D., P.A., T.L., D.S., L.I., C.S., L.K.M., C.L.G.; writing, C.E.W., D.H.D.G., M.-L.A.-L; supervision, T.P.S., D.H.D.G., M.-L.A.-L.; funding acquisition, C.E.W., C.L.G., M.-L.A.-L.

DECLARATION OF INTERESTS

C.S. acknowledges grant support from AstraZeneca, Boehringer-Ingelheim, Bristol-Myers Squibb, Pfizer, Roche-Ventana, Invitae (previously Archer Dx Inc–collaboration in minimal residual disease sequencing technologies), and Ono Pharmaceutical. C.S. is an AstraZeneca Advisory Board member and Chief Investigator for the AZ MeRmaiD 1 and 2 clinical trials and is also Co-Chief Investigator of the NHS Galleri trial funded by GRAIL and a paid member of GRAIL's SAB. He receives consultant fees from Achilles Therapeutics (also SAB member), Bicycle Therapeutics (also a SAB member), Genentech, Medicxi, Roche Innovation Centre– Shanghai, Metabomed (until July 2022), and the Sarah Cannon Research Institute. He had stock options in Apogen Biotechnologies and GRAIL until June 2021, and currently has stock options in Epic Bioscience, Bicycle Therapeutics, and has stock options and is co-founder of Achilles Therapeutics. C.S. is an inventor on a European patent application relating to assay technology to detect tumour recurrence (PCT/GB2017/053289), the patent has been licensed to commercial entities, and under his terms of employment, C.S. is due a revenue share of any revenue generated from such licence(s). C.S. holds patents relating to targeting neoantigens (PCT/EP2016/059401), identifying patient response to immune checkpoint blockade (PCT/EP2016/071471), determining HLA LOH (PCT/GB2018/052004), predicting survival rates of patients with cancer (PCT/GB2020/050221), identifying patients who respond to cancer treatment (PCT/GB2018/051912), a US patent relating to detecting tumour mutations (PCT/US2017/28013), methods for lung cancer detection (US20190106751A1) and both a European and US patent related to identifying insertion/deletion mutation targets (PCT/GB2018/051892) and is co-inventor to a patent application to determine methods and systems for tumour monitoring (PCT/EP2022/077987). C.S has received honoraria from Amgen, AstraZeneca, Pfizer, Novartis, GlaxoSmithKline, MSD, Bristol Myers Squibb, Illumina, and Roche-Ventana.

INCLUSION AND DIVERSITY

We support inclusive, diverse, and equitable conduct of research.

Received: July 18, 2022
Revised: February 5, 2023
Accepted: March 24, 2023
Published: May 8, 2023

REFERENCES

1. Schumacher, T.N., and Schreiber, R.D. (2015). Neoantigens in cancer immunotherapy. Science *348*, 69–74. https://doi.org/10.1126/science.aaa4971.

2. Dunn, G.P., Bruce, A.T., Ikeda, H., Old, L.J., and Schreiber, R.D. (2002). Cancer immunoediting: from immunosurveillance to tumor escape. Nat. Immunol. *3*, 991–998. https://doi.org/10.1038/ni1102-991.

3. Park, S.L., Buzzai, A., Rautela, J., Hor, J.L., Hochheiser, K., Effern, M., McBain, N., Wagner, T., Edwards, J., McConville, R., et al. (2019). Tissue-resident memory CD8$^+$ T cells promote melanoma–immune equilibrium in skin. Nature *565*, 366–371. https://doi.org/10.1038/s41586-018-0812-9.

4. Yoshida, K., Gowers, K.H.C., Lee-Six, H., Chandrasekharan, D.P., Coorens, T., Maughan, E.F., Beal, K., Menzies, A., Millar, F.R., Anderson, E., et al. (2020). Tobacco smoking and somatic mutations in human bronchial epithelium. Nature *578*, 266–272. https://doi.org/10.1038/s41586-020-1961-1.

5. Weeden, C.E., Chen, Y., Ma, S.B., Hu, Y., Ramm, G., Sutherland, K.D., Smyth, G.K., and Asselin-Labat, M.-L. (2017). Lung basal stem cells rapidly repair DNA damage using the error-prone nonhomologous end-joining pathway. PLoS Biol. *15*, e2000731. https://doi.org/10.1371/journal.pbio.2000731.

6. Domagala-Kulawik, J. (2008). Effects of cigarette smoke on the lung and systemic immunity. J. Physiol. Pharmacol. *59*, 19–34.

7. Campbell, J.D., Alexandrov, A., Kim, J., Wala, J., Berger, A.H., Pedamallu, C.S., Shukla, S.A., Guo, G., Brooks, A.N., Murray, B.A., et al. (2016). Distinct patterns of somatic genome alterations in lung adenocarcinomas and squamous cell carcinomas. Nat. Genet. *48*, 607–616. https://doi.org/10.1038/ng.3564.

8. Planchard, D., and Besse, B. (2015). Lung cancer in never-smokers. Eur. Respir. J. *45*, 1214–1217. https://doi.org/10.1183/09031936.00046915.

9. Li, B., Huang, X., and Fu, L. (2018). Impact of smoking on efficacy of PD-1/PD-L1 inhibitors in non-small cell lung cancer patients: a meta-analysis. Onco Targets Ther. *11*, 3691–3696. https://doi.org/10.2147/OTT.S156421.

10. Govindan, R., Ding, L., Griffith, M., Subramanian, J., Dees, N.D., Kanchi, K.L., Maher, C.A., Fulton, R., Fulton, L., Wallis, J., et al. (2012). Genomic landscape of non-small cell lung cancer in smokers and never-smokers. Cell *150*, 1121–1134. https://doi.org/10.1016/j.cell.2012.08.024.

11. Cho, W.C.S., Tan, K.T., Ma, V.W.S., Li, J.Y.C., Ngan, R.K.C., Cheuk, W., Yip, T.T.C., Yang, Y.-T., and Chen, S.-J. (2018). Targeted next-generation sequencing reveals recurrence-associated genomic alterations in early-stage non-small cell lung cancer. Oncotarget *9*, 36344–36357. https://doi.org/10.18632/oncotarget.26349.

12. Norum, J., and Nieder, C. (2018). Tobacco smoking and cessation and PD-L1 inhibitors in non-small cell lung cancer (NSCLC): a review of the literature. ESMO Open *3*, e000406. https://doi.org/10.1136/esmoopen-2018-000406.

13. Mueller, S.N., and Mackay, L.K. (2016). Tissue-resident memory T cells: local specialists in immune defence. Nat. Rev. Immunol. *16*, 79–89. https://doi.org/10.1038/nri.2015.3.

14. Sathaliyawala, T., Kubota, M., Yudanin, N., Turner, D., Camp, P., Thome, J.J.C., Bickham, K.L., Lerner, H., Goldstein, M., Sykes, M., et al. (2013). Distribution and compartmentalization of human circulating and tissue-resident memory T cell subsets. Immunity *38*, 187–197. https://doi.org/10.1016/j.immuni.2012.09.020.

15. Takamura, S., Kato, S., Motozono, C., Shimaoka, T., Ueha, S., Matsuo, K., Miyauchi, K., Masumoto, T., Katsushima, A., Nakayama, T., et al. (2019). Interstitial-resident memory CD8$^+$ T cells sustain frontline epithelial memory in the lung. J. Exp. Med. *216*, 2736–2747. https://doi.org/10.1084/jem.20190557.

16. Kumar, B.V., Connors, T.J., and Farber, D.L. (2018). Human T cell development, localization, and function throughout life. Immunity *48*, 202–213. https://doi.org/10.1016/j.immuni.2018.01.007.

17. Snyder, M.E., Finlayson, M.O., Connors, T.J., Dogra, P., Senda, T., Bush, E., Carpenter, D., Marboe, C., Benvenuto, L., Shah, L., et al. (2019). Generation and persistence of human tissue-resident memory T cells in lung transplantation. Sci. Immunol. *4*, eaav5581. https://doi.org/10.1126/sciimmunol.aav5581.

18. Marceaux, C., Weeden, C.E., Gordon, C.L., and Asselin-Labat, M.-L. (2021). Holding our breath: the promise of tissue-resident memory T cells in lung cancer. Transl. Lung Cancer Res. *10*, 2819–2829. https://doi.org/10.21037/tlcr-20-819.

19. Okła, K., Farber, D.L., and Zou, W. (2021). Tissue-resident memory T cells in tumor immunity and immunotherapy. J. Exp. Med. *218*, e20201605. https://doi.org/10.1084/jem.20201605.

20. Djenidi, F., Adam, J., Goubar, A., Durgeau, A., Meurice, G., de Montpréville, V., Validire, P., Besse, B., and Mami-Chouaib, F. (2015). CD8$^+$CD103$^+$ tumor-infiltrating lymphocytes are tumor-specific tissue-resident memory T cells and a prognostic factor for survival in lung cancer patients. J. Immunol. *194*, 3475–3486. https://doi.org/10.4049/jimmunol.1402711.

21. Oja, A.E., Piet, B., van der Zwan, D., Blaauwgeers, H., Mensink, M., de Kivit, S., Borst, J., Nolte, M.A., van Lier, R.A.W., Stark, R., et al. (2018). Functional heterogeneity of CD4$^+$ tumor-infiltrating lymphocytes with a resident memory phenotype in NSCLC. Front. Immunol. *9*, 2654. https://doi.org/10.3389/fimmu.2018.02654.

22. Ganesan, A.-P., Clarke, J., Wood, O., Garrido-Martin, E.M., Chee, S.J., Mellows, T., Samaniego-Castruita, D., Singh, D., Seumois, G., Alzetani, A., et al. (2017). Tissue-resident memory features are linked to the magnitude of cytotoxic T cell responses in human lung cancer. Nat. Immunol. *18*, 940–950. https://doi.org/10.1038/ni.3775.

23. Ariotti, S., Hogenbirk, M.A., Dijkgraaf, F.E., Visser, L.L., Hoekstra, M.E., Song, J.-Y., Jacobs, H., Haanen, J.B., and Schumacher, T.N. (2014). T cell memory. Skin-resident memory CD8$^+$ T cells trigger a state of tissue-wide pathogen alert. Science *346*, 101–105. https://doi.org/10.1126/science.1254803.

24. Schenkel, J.M., Fraser, K.A., Vezys, V., and Masopust, D. (2013). Sensing and alarm function of resident memory CD8$^+$ T cells. Nat. Immunol. *14*, 509–513. https://doi.org/10.1038/ni.2568.

25. Menares, E., Gálvez-Cancino, F., Cáceres-Morgado, P., Ghorani, E., López, E., Díaz, X., Saavedra-Almarza, J., Figueroa, D.A., Roa, E., Quezada, S.A., et al. (2019). Tissue-resident memory CD8$^+$ T cells amplify anti-tumor immunity by triggering antigen spreading through dendritic cells. Nat. Commun. *27*, 4401. https://doi.org/10.1038/s41467-019-12319-x.

26. Simoni, Y., Becht, E., Fehlings, M., Loh, C.Y., Koo, S.-L., Teng, K.W.W., Yeong, J.P.S., Nahar, R., Zhang, T., Kared, H., et al. (2018). Bystander CD8$^+$ T cells are abundant and phenotypically distinct in human tumour infiltrates. Nature *557*, 575–579. https://doi.org/10.1038/s41586-018-0130-2.

27. Chow, A., Uddin, F.Z., Liu, M., Dobrin, A., Nabet, B.Y., Mangarin, L., Lavin, Y., Rizvi, H., Tischfield, S.E., Quintanal-Villalonga, A., et al. (2023). The ectonucleotidase CD39 identifies tumor-reactive CD8$^+$ T cells predictive of immune checkpoint blockade efficacy in human lung cancer. Immunity *56*, 93–106.e6. https://doi.org/10.1016/j.immuni.2022.12.001.

28. Hanahan, D., and Weinberg, R.A. (2011). Hallmarks of cancer: the next generation. Cell *144*, 646–674. https://doi.org/10.1016/j.cell.2011.02.013.

29. Schreiber, R.D., Old, L.J., and Smyth, M.J. (2011). Cancer immunoediting: integrating immunity's roles in cancer suppression and promotion. Science *331*, 1565–1570. https://doi.org/10.1126/science.1203486.

30. Kalbasi, A., and Ribas, A. (2020). Tumour-intrinsic resistance to immune checkpoint blockade. Nat. Rev. Immunol. *20*, 25–39. https://doi.org/10.1038/s41577-019-0218-4.

31. Anagnostou, V., Smith, K.N., Forde, P.M., Niknafs, N., Bhattacharya, R., White, J., Zhang, T., Adleff, V., Phallen, J., Wali, N., et al. (2017). Evolution of neoantigen landscape during immune checkpoint blockade in non-small cell lung cancer. Cancer Discov. *7*, 264–276. https://doi.org/10.1158/2159-8290.CD-16-0828.

32. Lakatos, E., Williams, M.J., Schenck, R.O., Cross, W.C.H., Househam, J., Zapata, L., Werner, B., Gatenbee, C., Robertson-Tessi, M., Barnes, C.P., et al. (2020). Evolutionary dynamics of neoantigens in growing tumors. Nat. Genet. *52*, 1057–1066. https://doi.org/10.1038/s41588-020-0687-1.

33. Chen, L., and Flies, D.B. (2013). Molecular mechanisms of T cell co-stimulation and co-inhibition. Nat. Rev. Immunol. *13*, 227–242. https://doi.org/10.1038/nri3405.

34. Lavin, Y., Kobayashi, S., Leader, A., Amir, E.-A.D., Elefant, N., Bigenwald, C., Remark, R., Sweeney, R., Becker, C.D., Levine, J.H., et al. (2017). Innate immune landscape in early lung adenocarcinoma by paired single-cell analyzes. Cell *169*, 750–765.e17. https://doi.org/10.1016/j.cell.2017.04.014.

35. Corgnac, S., Malenica, I., Mezquita, L., Auclin, E., Voilin, E., Kacher, J., Halse, H., Grynszpan, L., Signolle, N., Dayris, T., et al. (2020). $CD103^{+}CD8^{+}$ TRM cells accumulate in tumors of anti-PD-1-responder lung cancer patients and are tumor-reactive lymphocytes enriched with Tc17. Cell Rep. Med. *1*, 100127. https://doi.org/10.1016/j.xcrm.2020.100127.

36. Jamal-Hanjani, M., Wilson, G.A., Mcgranahan, N., Birkbak, N.J., Watkins, T.B.K., Veeriah, S., Shafi, S., Johnson, D.H., Mitter, R., Rosenthal, R., et al. (2017). Tracking the evolution of non–small-cell lung cancer. N. Engl. J. Med. *376*, 2109–2121. https://doi.org/10.1056/NEJMoa1616288.

37. Devarakonda, S., Li, Y., Martins Rodrigues, F., Sankararaman, S., Kadara, H., Goparaju, C., Lanc, I., Pepin, K., Waqar, S.N., Morgensztern, D., et al. (2021). Genomic profiling of lung adenocarcinoma in never-smokers. J. Clin. Oncol. *39*, 3747–3758. https://doi.org/10.1200/JCO.21.01691.

38. Ge, C., Monk, I.R., Pizzolla, A., Wang, N., Bedford, J.G., Stinear, T.P., Westall, G.P., and Wakim, L.M. (2019). Bystander activation of pulmonary Trm cells attenuates the severity of bacterial pneumonia by enhancing neutrophil recruitment. Cell Rep. *29*, 4236–4244.e3. https://doi.org/10.1016/j.celrep.2019.11.103.

39. Burr, M.L., Sparbier, C.E., Chan, K.L., Chan, Y.-C., Kersbergen, A., Lam, E.Y.N., Azidis-Yates, E., Vassiliadis, D., Bell, C.C., Gilan, O., et al. (2019). An evolutionarily conserved function of polycomb silences the MHC class I antigen presentation pathway and enables immune evasion in cancer. Cancer Cell *36*, 385–401.e8. https://doi.org/10.1016/j.ccell.2019.08.008.

40. Paz-Ares, L.G., Ramalingam, S.S., Ciuleanu, T.-E., Lee, J.-S., Urban, L., Caro, R.B., Park, K., Sakai, H., Ohe, Y., Nishio, M., et al. (2022). First-line nivolumab plus ipilimumab in advanced NSCLC: 4-year outcomes from the randomized, open-label, phase 3 CheckMate 227 Part 1 trial. J. Thorac. Oncol. *17*, 289–308. https://doi.org/10.1016/j.jtho.2021.09.010.

41. Chen, H., Carrot-Zhang, J., Zhao, Y., Hu, H., Freeman, S.S., Yu, S., Ha, G., Taylor, A.M., Berger, A.C., Westlake, L., et al. (2019). Genomic and immune profiling of pre-invasive lung adenocarcinoma. Nat. Commun. *29*, 5472. https://doi.org/10.1038/s41467-019-13460-3.

42. Leong, T.L., Gayevskiy, V., Steinfort, D.P., De Massy, M.R., Gonzalez-Rajal, A., Marini, K.D., Stone, E., Chin, V., Havryk, A., Plit, M., et al. (2019). Deep multi-region whole-genome sequencing reveals heterogeneity and gene-by-environment interactions in treatment-naive, metastatic lung cancer. Oncogene *38*, 1661–1675. https://doi.org/10.1038/s41388-018-0536-1.

43. Nahar, R., Zhai, W., Zhang, T., Takano, A., Khng, A.J., Lee, Y.Y., Liu, X., Lim, C.H., Koh, T.P.T., Aung, Z.W., et al. (2018). Elucidating the genomic architecture of Asian EGFR-mutant lung adenocarcinoma through multi-region exome sequencing. Nat. Commun *9*, 216. https://doi.org/10.1038/s41467-017-02584-z.

44. Koebel, C.M., Vermi, W., Swann, J.B., Zerafa, N., Rodig, S.J., Old, L.J., Smyth, M.J., and Schreiber, R.D. (2007). Adaptive immunity maintains occult cancer in an equilibrium state. Nature *450*, 903–907. https://doi.org/10.1038/nature06309.

45. Quaglino, P., Marenco, F., Osella-Abate, S., Cappello, N., Ortoncelli, M., Salomone, B., Fierro, M.T., Savoia, P., and Bernengo, M.G. (2010). Vitiligo is an independent favourable prognostic factor in stage III and IV metastatic melanoma patients: results from a single-institution hospital-based observational cohort study. Ann. Oncol. *21*, 409–414. https://doi.org/10.1093/annonc/mdp325.

46. Teulings, H.-E., Limpens, J., Jansen, S.N., Zwinderman, A.H., Reitsma, J.B., Spuls, P.I., and Luiten, R.M. (2015). Vitiligo-like depigmentation in patients with stage III-IV melanoma receiving immunotherapy and its association with survival: a systematic review and meta-analysis. J. Clin. Oncol. *33*, 773–781. https://doi.org/10.1200/JCO.2014.57.4756.

47. Malik, B.T., Byrne, K.T., Vella, J.L., Zhang, P., Shabaneh, T.B., Steinberg, S.M., Molodtsov, A.K., Bowers, J.S., Angeles, C.V., Paulos, C.M., et al. (2017). Resident memory T cells in the skin mediate durable immunity to melanoma. Sci. Immunol. *14*, eaam6346. https://doi.org/10.1126/sciimmunol.aam6346.

48. Katki, H.A., Kovalchik, S.A., Berg, C.D., Cheung, L.C., and Chaturvedi, A.K. (2016). Development and validation of risk models to select ever-smokers for CT lung cancer screening. JAMA *315*, 2300–2311. https://doi.org/10.1001/jama.2016.6255.

49. Teixeira, V.H., Pipinikas, C.P., Pennycuick, A., Lee-Six, H., Chandrasekharan, D., Beane, J., Morris, T.J., Karpathakis, A., Feber, A., Breeze, C.E., et al. (2019). Deciphering the genomic, epigenomic, and transcriptomic landscapes of pre-invasive lung cancer lesions. Nat. Med. *25*, 517–525. https://doi.org/10.1038/s41591-018-0323-0.

50. Pennycuick, A., Teixeira, V.H., AbdulJabbar, K., Raza, S.E.A., Lund, T., Akarca, A.U., Rosenthal, R., Kalinke, L., Chandrasekharan, D.P., Pipinikas, C.P., et al. (2020). Immune surveillance in clinical regression of pre-invasive squamous cell lung cancer. Cancer Discov. *10*, 1489–1499. https://doi.org/10.1158/2159-8290.CD-19-1366.

51. Mascaux, C., Angelova, M., Vasaturo, A., Beane, J., Hijazi, K., Anthoine, G., Buttard, B., Rothe, F., Willard-Gallo, K., Haller, A., et al. (2019). Immune evasion before tumour invasion in early lung squamous carcinogenesis. Nature *571*, 570–575. https://doi.org/10.1038/s41586-019-1330-0.

52. Dejima, H., Hu, X., Chen, R., Zhang, J., Fujimoto, J., Parra, E.R., Haymaker, C., Hubert, S.M., Duose, D., Solis, L.M., et al. (2021). Immune evolution from preneoplasia to invasive lung adenocarcinomas and underlying molecular features. Nat. Commun. *11*, 2722. https://doi.org/10.1038/s41467-021-22890-x.

53. Savas, P., Virassamy, B., Ye, C., Salim, A., Mintoff, C.P., Caramia, F., Salgado, R., Byrne, D.J., Teo, Z.L., Dushyanthen, S., et al. (2018). Single-cell profiling of breast cancer T cells reveals a tissue-resident memory subset associated with improved prognosis. Nat. Med. *24*, 986–993. https://doi.org/10.1038/s41591-018-0078-7.

54. Sharma, P., Hu-Lieskovan, S., Wargo, J.A., and Ribas, A. (2017). Primary, adaptive, and acquired resistance to cancer immunotherapy. Cell *168*, 707–723. https://doi.org/10.1016/j.cell.2017.01.017.

55. Montesion, M., Murugesan, K., Jin, D.X., Sharaf, R., Sanchez, N., Guria, A., Minker, M., Li, G., Fisher, V., Sokol, E.S., et al. (2021). Somatic HLA class I loss is a widespread mechanism of immune evasion which refines the use of tumor mutational burden as a biomarker of checkpoint inhibitor response. Cancer Discov. *11*, 282–292. https://doi.org/10.1158/2159-8290.CD-20-0672.

56. Mcgranahan, N., Rosenthal, R., Hiley, C.T., Rowan, A.J., Watkins, T.B.K., Wilson, G.A., Birkbak, N.J., Veeriah, S., Van Loo, P., Herrero, J., et al. (2017). Allele-specific HLA loss and immune escape in lung cancer evolution. Cell *171*, 1259–1271.e11. https://doi.org/10.1016/j.cell.2017.10.001.

57. Joshi, K., De Massy, M.R., Ismail, M., Reading, J.L., Uddin, I., Woolston, A., Hatipoglu, E., Oakes, T., Rosenthal, R., Peacock, T., et al. (2019). Spatial heterogeneity of the T cell receptor repertoire reflects the mutational landscape in lung cancer. Nat. Med. *25*, 1549–1559. https://doi.org/10.1038/s41591-019-0592-2.

58. Passaro, A., Attili, I., Morganti, S., Del Signore, E., Gianoncelli, L., Spitaleri, G., Stati, V., Catania, C., Curigliano, G., and de Marinis, F. (2020). Clinical features affecting survival in metastatic NSCLC treated with immunotherapy: a critical review of published data. Cancer Treat Rev. *89*, 102085. https://doi.org/10.1016/j.ctrv.2020.102085.

59. Supabphol, S., Li, L., Goedegebuure, S.P., and Gillanders, W.E. (2021). Neoantigen vaccine platforms in clinical development: understanding the future of personalized immunotherapy. Expert Opin. Investig. Drugs *30*, 529–541. https://doi.org/10.1080/13543784.2021.1896702.

60. Simpson, T.R., Li, F., Montalvo-Ortiz, W., Sepulveda, M.A., Bergerhoff, K., Arce, F., Roddie, C., Henry, J.Y., Yagita, H., Wolchok, J.D., et al. (2013).

Fc-dependent depletion of tumor-infiltrating regulatory T cells co-defines the efficacy of anti-CTLA-4 therapy against melanoma. J. Exp. Med. *210*, 1695–1710. https://doi.org/10.1084/jem.20130579.

61. Robbins, P.F., Lu, Y.-C., El-Gamil, M., Li, Y.F., Gross, C., Gartner, J., Lin, J.C., Teer, J.K., Cliften, P., Tycksen, E., et al. (2013). Mining exomic sequencing data to identify mutated antigens recognized by adoptively transferred tumor-reactive T cells. Nat. Med. *19*, 747–752. https://doi.org/10.1038/nm.3161.
62. Desai, R., Coxon, A.T., and Dunn, G.P. (2022). Therapeutic applications of the cancer immunoediting hypothesis. Semin. Cancer Biol. *78*, 63–77. https://doi.org/10.1016/j.semcancer.2021.03.002.
63. Sharma, V.J., Starkey, G., D'Costa, R., James, F., Mouhtouris, E., Davis, L., Wang, B.Z., Vago, A., Raman, J., Mackay, L.K., et al. (2023). Australian donation and transplantation Biobank: a research Biobank integrated within a deceased organ and tissue donation program. Transplant. Direct *9*, e1422. https://doi.org/10.1097/TXD.0000000000001422.
64. Best, S.A., Ding, S., Kersbergen, A., Dong, X., Song, J.-Y., Xie, Y., Reljic, B., Li, K., Vince, J.E., Rathi, V., et al. (2019). Distinct initiating events underpin the immune and metabolic heterogeneity of KRAS-mutant lung adenocarcinoma. Nat. Commun. *10*, 4190. https://doi.org/10.1038/s41467-019-12164-y.
65. Gebhardt, T., Wakim, L.M., Eidsmo, L., Reading, P.C., Heath, W.R., and Carbone, F.R. (2009). Memory T cells in nonlymphoid tissue that provide enhanced local immunity during infection with herpes simplex virus. Nat. Immunol. *10*, 524–530. https://doi.org/10.1038/ni.1718.
66. Bankhead, P., Loughrey, M.B., Fernández, J.A., Dombrowski, Y., McArt, D.G., Dunne, P.D., McQuaid, S., Gray, R.T., Murray, L.J., Coleman, H.G., et al. (2017). QuPath: open source software for digital pathology image analysis. Sci. Rep. *7*, 16878. https://doi.org/10.1038/s41598-017-17204-5.
67. Schmidt, U., Weigert, M., Broaddus, C., and Meyers, G. (2018). Cell detection with star-convex polygons. Preprint at arXiv. https://doi.org/10.1007/978-3-030-00934-2_30.
68. Rahman, A.H., Tordesillas, L., and Berin, M.C. (2016). Heparin reduces nonspecific eosinophil staining artifacts in mass cytometry experiments. Cytometry A. *89*, 601–607. https://doi.org/10.1002/cyto.a.22826.
69. Crowell, H.L., Chevrier, S., Jacobs, A., Sivapatham, S., Tumor Profiler Consortium, Bodenmiller, B., and Robinson, M.D. (2020). An R-based reproducible and user-friendly preprocessing pipeline for CyTOF data. F1000Res. *9*, 1263. https://doi.org/10.12688/f1000research.26073.1.
70. Amir, E.-A.D., Davis, K.L., Tadmor, M.D., Simonds, E.F., Levine, J.H., Bendall, S.C., Shenfeld, D.K., Krishnaswamy, S., Nolan, G.P., and Pe'er, D. (2013). viSNE enables visualization of high dimensional single-cell data and reveals phenotypic heterogeneity of leukemia. Nat. Biotechnol. *31*, 545–552. https://doi.org/10.1038/nbt.2594.
71. Ritchie, M.E., Phipson, B., Wu, D., Hu, Y., Law, C.W., Shi, W., and Smyth, G.K. (2015). Limma powers differential expression analyzes for RNA-sequencing and microarray studies. Nucleic Acids Res. *43*, e47. https://doi.org/10.1093/nar/gkv007.
72. Hoadley, K.A., Yau, C., Hinoue, T., Wolf, D.M., Lazar, A.J., Drill, E., Shen, R., Taylor, A.M., Cherniack, A.D., Thorsson, V., et al. (2018). Cell-of-Origin patterns dominate the molecular classification of 10,000 tumors from 33 types of cancer. Cell *173*, 291–304.e6. https://doi.org/10.1016/j.cell.2018.03.022.
73. Rooney, M.S., Shukla, S.A., Wu, C.J., Getz, G., and Hacohen, N. (2015). Molecular and genetic properties of tumors associated with local immune cytolytic activity. Cell *160*, 48–61. https://doi.org/10.1016/j.cell.2014.12.033.
74. Liao, Y., Smyth, G.K., and Shi, W. (2014). featureCounts: an efficient general purpose program for assigning sequence reads to genomic features. Bioinformatics *30*, 923–930. https://doi.org/10.1093/bioinformatics/btt656.
75. Molania, R., Foroutan, M., Gagnon-Bartsch, J.A., Gandolfo, L.C., Jain, A., Sinha, A., Olshansky, G., Dobrovic, A., Papenfuss, A.T., and Speed, T.P. (2023). Removing unwanted variation from large-scale RNA sequencing data with PRPS. Nat. Biotechnol. *41*, 82–95. https://doi.org/10.1038/s41587-022-01440-w.
76. Foroutan, M., Bhuva, D.D., Lyu, R., Horan, K., Cursons, J., and Davis, M.J. (2018). Single sample scoring of molecular phenotypes. BMC Bioinformatics *19*, 404–410. https://doi.org/10.1186/s12859-018-2435-4.
77. Shukla, S.A., Rooney, M.S., Rajasagi, M., Tiao, G., Dixon, P.M., Lawrence, M.S., Stevens, J., Lane, W.J., Dellagatta, J.L., Steelman, S., et al. (2015). Comprehensive analysis of cancer-associated somatic mutations in class I HLA genes. Nat. Biotechnol. *33*, 1152–1158. https://doi.org/10.1038/nbt.3344.

STAR★METHODS

KEY RESOURCES TABLE

REAGENT or RESOURCE	SOURCE	IDENTIFIER
Antibodies		
Anti-Human EpCam, clone 9C4	Fluidigm	Cat# 3141006B; RRID: AB_2687653
Anti-Human Pan keratin, clone C11	Fluidigm	Cat# 3162027A; RRID: AB_283075
Anti-Human p63*, clone EPR5701	Abcam	Cat# ab214790; RRID: AB_10971840*
Anti-Human TTF1*, clone EP1584Y	Abcam	Cat# ab216648; RRID: AB_1310784*
Anti-Human HLA-A,B,C*, clone W6/32	WEHI	N/A
Anti-Human CD45, clone HI30	Fluidigm	Cat# 3089003B; RRID: AB_2661851
Anti-Human CD11a, clone H111	Fluidigm	Cat# 3142006B; RRID: AB_2877095
Anti-Human CD16, clone 3G8	Fluidigm	Cat# 3209002B; RRID: AB_3142006B
Anti-Human NKp46*, clone 9E2	Biolegend	Cat# 331902; RRID: AB_1027637
Anti-Human HLA-DR*, clone L243	Biolegend	Cat# 307602; RRID: AB_314680
Anti-Human CD3*, clone UCHT1	Biolegend	Cat# 300443; RRID: AB_2562808
Anti-Human CD4, clone RPA-T4	Fluidigm	Cat# 3145001B; RRID: AB_2661789
Anti-Human CD8a, clone RPA-T8	Fluidigm	Cat# 3146001B; RRID: AB_2687641
Anti-Human CD127, clone A019D5	Fluidigm	Cat# 3176004B; RRID: AB_2687863
Anti-Human CD25, clone 2A3	Fluidigm	Cat# 3169003B; RRID: AB_2661806
Anti-Human CD45RO, clone UCHL1	Fluidigm	Cat# 3149001B; RRID: AB_2687851
Anti-Human CD45RA, clone HI100	Fluidigm	Cat# 3143006B; RRID: AB_2651156
Anti-Human CCR7, clone G043H7	Fluidigm	Cat# 3159003A; RRID: AB_2714155
Anti-Human CD69, clone FN50	Fluidigm	Cat# 3144018B; RRID: AB_2687849
Anti-Human TBET, clone 4B10	Fluidigm	Cat# 3161014B; RRID: AB_2858233
Anti-Human CD28, clone CD28.2	Fluidigm	Cat# 3160003B; RRID: AB_2868400
Anti-Human 4-1BB*, clone 4B4-1	Biolegend	Cat# 309802; RRID: AB_314781
Anti-Human OX40*, clone ACT35	Biolegend	Cat# 350015; RRID: AB_2563718
Anti-Human CD27, clone L128	Fluidigm	Cat# 3167006B; RRID: AB_2811093
Anti-Human ICOS, clone C398.4A	Fluidigm	Cat# 3148019B; RRID: AB_2756435
Anti-Human CTLA-4, clone 14D3	Fluidigm	Cat# 3170005B; RRID: AB_2858238
Anti-Human PD-1, clone EH12.2H7	Fluidigm	Cat# 3155009B; RRID: AB_2811087
Anti-Human CD57, clone HCD57	Fluidigm	Cat# 3163022B; RRID: AB_2756434
Anti-Human Lag3*, clone 11C3C65	Biolegend	Cat# 369302; RRID: AB_2616876
Anti-Human Tim3, clone F38-2E2	Fluidigm	Cat# 3153008B; RRID: AB_2687644
Anti-Human Ki67, clone B56	Fluidigm	Cat# 3168007B; RRID: AB_2800467
Anti-Human ICOS, clone C398.4A	BD	Cat# 565881; RRID: AB_2744480
Anti-Human CD45, clone H130	eBioscience	Cat# 58-0459-42; RRID: AB_11218673
Anti-Human CD45, clone HI30	BD	Cat# 563204; RRID: AB_2738067
Anti-Human PD1, clone EH12.2H7	Biolegend	Cat# 329906; RRID: AB_940483
Anti-Human CD103, clone BERact8	biolegend	Cat# 350224; RRID: AB_2716189
Anti-Human CD4, clone OKT4	Biolegend	Cat# 317412; RRID: AB_571957
Anti-Human CD4, clone OKT4	Biolegend	Cat# 317428; RRID: AB_1186122
Anti-Human CD8, clone SK1	Biolegend	Cat# 344710; RRID: AB_2044010
Anti-Human CD8, clone SK1	Biolegend	Cat# 344718; RRID: AB_10551438
Anti-Human HLA-A,B,C, clone W6/32	eBioscience	Cat# 46-9983-42; RRID: AB_10804486
Anti-Human CTLA4, clone 14D3	eBioscience	Cat# 25-1529-42; RRID: AB_2573406
Anti-Human 41BB, clone 4B4-1	Biolegend	Cat# 309810; RRID: AB_830672
Anti-Human CD69, clone FN50	BD	Cat# 565155; RRID: AB_2744449

(*Continued on next page*)

Continued

REAGENT or RESOURCE	SOURCE	IDENTIFIER
Anti-Human EpCAM, clone 9C4	Stem Cell Technologies	Cat# 10109; RRID: AB_215530
Anti-Human CD45RA, clone HI100	Biolegend	Cat# 304128; RRID: AB_10708880
Anti-Human OX40, clone BER-ACT35	BD	Cat# 746649; RRID: AB_2743926
Anti-Human CD3, clone UCHT1	Biolegend	Cat# 300436; RRID: AB_2562124
Anti-Human CD25, clone BC96	Biolegend	Cat# 302632; RRID: AB_11218989
Anti-Human CCR7, clone G043H7	Biolegend	Cat# 353234; RRID: AB_2563867
Anti-Human CD27, clone L128	BD	Cat# 747310; RRID: AB_2872019
Anti-Human HLA-DR, clone L243	Biolegend	Cat# 307642; RRID: AB_2563461
Anti-Human CD235a, clone GA-R2	BD	Cat# 555570; RRID: AB_395949
Anti-Human CD140b, clone 28D4	BD	Cat# 558821; RRID: AB_397132
Anti-Human CD31, clone WM59	BD	Cat# 555446; RRID: AB_395839
Anti-Human CTLA4, clone 14D3	eBioscience	Cat# 25-1529-42; RRID: AB_2573406
Anti-Human Foxp3, clone 206D	Biolegend	Cat# 320124; RRID: AB_2565972
Anti-Human Ki67, clone B56	BD	Cat# 561281; RRID: AB_10613816
Anti-Human Granzyme B, clone GB11	BD	Cat# 563388; RRID: AB_2738174
Anti-Human Perforin, clone dG9	Biolegend	Cat# 308130; RRID: AB_2687190
Anti-Mouse CD45.1, clone A20	Biolegend	Cat# 110713; RRID: AB_313502
Anti-Mouse CD45.2, clone 104	BD	Cat# 564616; RRID: AB_2738867
Anti-Mouse TCRaV2, clone B20.1	Biolegend	Cat# 127808; RRID: AB_1134183
Anti-Mouse CD3, clone 17A2	eBioscience	Cat# 58-0032-82; RRID: AB_11217479
Anti-Mouse CD4, clone GK1.5	BD	Cat# 612761; RRID: AB_2870092
Anti-Mouse CD8a, clone 53–6.7	Biolegend	Cat# 100742; RRID: AB_2563056
Anti-Mouse CD44, clone IM7	Biolegend	Cat# 103026; RRID: AB_493713
Anti-Mouse CD62L, clone MEL-14	Biolegend	Cat# 104428; RRID: AB_830799
Anti-Mouse CD25, clone PC61	Biolegend	Cat# 102042; RRID: AB_2562270
Anti-Mouse ICOS, clone 7E.17G9	eBioscience	Cat# 46-9942-82; RRID: AB_2744728
Anti-Mouse PD1, clone 29F1A12	Biolegend	Cat# 135219; RRID: AB_11125371
Anti-Mouse CD69, clone H1.2F3	Biolegend	Cat# 104537; RRID: AB_2566120
Anti-Mouse CD103, clone 2E7	Biolegend	Cat# 121421; RRID: AB_10900074
Anti-Mouse Foxp3, clone FJK-16S	eBioscience	Cat# 48-5773-82; RRID: AB_1518812
Anti-Mouse Granzyme B, clone QA16A02	Biolegend	Cat# 372214; RRID: AB_2728381
Anti-Mouse H-2Kb, clone AF6-88.5	Biolegend	Cat# 116510; RRID: AB_492915
Anti-Mouse IFNγ, clone XMG1.2	Biolegend	Cat# 505816; RRID: AB_493315
Anti-Mouse Ki67, clone B56	BD	Cat# 563756; RRID: AB_2732007
Anti-Mouse NK-p46, clone 29A1.4	eBiosciences	Cat# 746875; RRID: AB_2871675
Anti-Mouse OVA-tet, clone N/A	NIH tetramer core facility	N/A
Anti-Human panCK, clone AE1/AE3	Abcam	Cat# ab27988; RRID: AB_777047
Anti-Human CD8, clone SP16	Invitrogen	Cat# MA5-14548; RRID: AB_10984334
Anti-Human CD69, clone EPR21814	Abcam	Cat# ab233396; RRID: AB_2922929
Anti-Human CD103, clone EPR4166(2)	Abcam	Cat# ab129202; RRID: AB_11142856
Anti-Human CD39, clone EPR20627	Abcam	Cat# ab223842; RRID: AB_2889212
Anti-Human PD1, clone NAT105	Abcam	Cat# ab52587; RRID: AB_881954
Anti-Mouse CD8a, clone polyclonal	SySy	Cat# HS-361003
Anti-Mouse Ki67, clone D3B5	CST	Cat# 12202; RRID: AB_2620142
Anti-Mouse OVA-H2Kb, clone 25-D1.16	eBiosciences	Cat# 12-5743-82; RRID: AB_925774
Anti-Mouse NK1.1, clone PK136	WEHI monoclonal lab	N/A
Anti-Mouse CD11c, clone N418	WEHI monoclonal lab	N/A
Anti-Mouse Phospho-STAT1, clone 58D6	Cell signaling	Cat# 9167; RRID: AB_561284
Anti-Mouse IFNγ, clone XMG1.2	WEHI monoclonal lab	N/A

(*Continued on next page*)

Continued

REAGENT or RESOURCE	SOURCE	IDENTIFIER
Bacterial and virus strains		
Ad5 CMV-cre	University of Iowa Gene Transfer Core	Cat# VVC-U of Iowa-5
Chemicals, peptides, and recombinant proteins		
Anti-mouse PD-1, clone RMP1-14	BioXCell	cat# BE0146
Anti-mouse CTLA4, clone UC10-4F10-11	BioXCell	cat# BP0032
Rat IgG2a isotype control, Clone 2A	BioXCell	cat# BE0089
Armenian Hamster IgG isotype control, HTK888	Biolegend	Cat# 400966
SIINFEKL-MHC Tetramer Alexa 568	NIH Tetramer Core Facility	N/A
Recombinant mouse IFNg protein	ABCAM	Ab123747
Deposited data		
TRACERx	Jamal-Hanjani et al.[36]	EGAD00001003206
LxG	Leong et al.[42]	EGAS00001003830
Chen	Chen et al.[41]	EGAD00001005479
Nahar	Nahar et al., 2018[43]	EGAS00001001736
Experimental models: Organisms/strains		
Mouse: *Kras^{G12D}/p53 $^{fl/fl}$*	The Jackson Laboratory	LSL-K-ras G12D; B6.129S4-KrastmTyj/J, p53 floxed; B6.129P2-Trp53tm1Brn/J
Biological samples		
Patient samples	Victorian Cancer Biobank Australian Donation and Transplant Biobank	N/A
Software and algorithms		
GraphPad Prism 7	GraphPad Software	https://www.graphpad.com/scientific-software/prism/
FlowJo	FlowJo LLC	https://www.flowjo.com/solutions/flowjo
QuPath	Bankhead et al.[66]	https://qupath.github.io/

RESOURCE AVAILABILITY

Lead contact

Further information and requests for reagents and resources should be directed and will be fulfilled by the Contact: M-L. Asselin-Labat: labat@wehi.edu.au.

Materials availability

This study did not generate new unique reagents.

Data and code availability

The datasets analyzed during the current study are available in the EGA repository:

TRACERx; https://ega-archive.org/datasets/EGAD00001003206.
LxG; https://ega-archive.org/studies/EGAS00001003830.
Chen; https://ega-archive.org/datasets/EGAD00001005479.
Nahar; https://ega-archive.org/studies/EGAS00001001736.
Data used in summary figures (Figures 1C, 1E, 2A–2C, 2F, 5B–5E, S1D, S4E–S4J and S8A) are contained in Table S4.
Code to quantify Ki67^{+}CD8^{+} cells in immunostained sections is available at https://github.com/WEHI-labatlab/TRM-paper.

EXPERIMENTAL MODEL AND SUBJECT DETAILS

Patient samples

Written informed consent was obtained from all lung cancer patients by the Victorian Cancer Biobank or the Australian Donation and Transplant Biobank prior to inclusion in the study, according to protocols approved by the WEHI Human Research Ethics Committee (HREC, approval #10/04). Patients were classified as ever-smokers (current and ex-smokers who had quit smoking at least 1 year

prior to sample collection) or never-smokers (lifetime smoking of less than 100 cigarettes). Matched tumor and adjacent normal lung specimens confirmed by histology were obtained through the Victorian Cancer Biobank from surgically resected tissue of early-stage lung cancer patients (Stage I to IIIa). Primary tumor samples from patients with unresectable, late-stage lung cancers were obtained from endobronchial ultrasound biopsies (EBUS), as was a sample of pulmonary lymph node containing metastatic cancer cells used as a reference control for CyTOF. Human tissues from non-cancer patients were obtained from deceased organ donors at the time of organ acquisition for transplantation through the Australian Donation and Transplant Biobank[63] (HREC/4814/Austin-2019). All donors were free of cancer, hepatitis B, and hepatitis C, and were HIV negative. Patient and organ donor details are described in Tables S1 and S2, all cancer patients were treatment-naive. Healthy PBMC used as a reference control was collected from a patient through the Victorian Blood Donor Registry (WEHI HREC approval # 2016.066; Melbourne Health HREC/16/MH/62). Written informed consent was obtained.

Kras$^{G12D/+}$;*p53*$^{flox/flox}$-OVA murine lung cancer cell line

The *Kras*$^{G12D/+}$;*p53*$^{flox/flox}$ (KP) murine tumor cell line was established from tumor arising in *Kras*$^{G12D/+}$;*p53*$^{flox/flox}$ mice following intranasal infection with Ad5-CMV-Cre[64] (University of Iowa Gene Transfer Core Facility). Cells were grown in DMEM F12 + Glutamax (Gibco) 10% FCS/FBS, Penicillin (100U/mL)/Streptomycin (100ug/mL) (Gibco), 0.04 mg/mL hydrocortisone (Sigma-Aldrich), 1x Insulin-Transferrin-Selenium (Gibco), 5 ng/mL mouse EGF (Gibco) in normoxic, 5% CO2 incubator. KP-OVA mCherry line was generated by transduction of KP cells with retroviral vectors MSCV-OVA-IRES Cherry sequence[39] (a gift from Marian Burr and Mark Dawson). To confirm H-2Kb and OVA- H-2KB expression *in vitro*, KP-OVA cells were treated 48 h with murine IFNγ (10 ng/mL). Cells were then trypsinised and stained with H-2Kb-A488 or OVA-H-2Kb-PE antibody for analysis by flow cytometry.

Mice

All animal experiments were approved by the WEHI Animal Ethics Committee (Approval #2020.001; 2020.002; 2020.026) and the University of Melbourne Ethics Committee and conducted in accordance with the National Health and Medical Research Council Australian Code of Practice for the Care and Use of Animals for Scientific Purposes. C57B/6 mice were bred and maintained in WEHI animal facilities according to institutional requirements. gBT-I, gBT-I × B6.SJL-PtprcaPep3b/BoyJ (gBT-I.CD45.1), OT-I × B6.SJL-PtprcaPep3b/BoyJ (OT-I.CD45.1) were bred in the Department of Microbiology and Immunology, The University of Melbourne. Male and female mice aged eight to ten weeks were used in the experiments. The investigators did not perform any experiments in blind.

METHOD DETAILS

In vivo formation of T_{RM} and lung tumors

For T_{RM} formation, *in vitro* activated CD8$^+$ T cells from transgenic gBT-I.CD45.1, or OT-I.CD45.1 T cells were activated *in vitro* for 4–5 days with gB498–505 (SSIEFARL) or OVA257–264 (SIINFEKL) peptide-pulsed splenocytes in the presence of recombinant human interleukin (IL)-2 (25 units per mL, Peprotech), as described.[65] C57/B6 mice were injected intravenously with 5.10^6 effector gBT-I or OT-I cells and intranasally with poly:IC (25 μg/mouse Tocris Biosciences) and gB or OVA peptide (1 μg/mouse). Mice were injected intravenously with 2.5.10^5 kP-OVA cells 14 days later and collected after 8 weeks later. To label circulating T cells, mice were injected i.v. with 1.5 μg of anti-CD3-AF532 antibody 3 min prior to euthanasia. Left lung lobes, liver, kidney and spleen were taken for flow cytometry analyzes and right lung lobes were inflated in 4% PFA for histological analyzes.

Quantification of tumor burden and multiplex immunostaining

Tumor burden was quantified in QuPath[66] on H&E sections by training pixel classifiers using manual annotation of tumor and lung tissues. For OPAL staining analysis, tissues were selected using Phenochart software (PerkinElmer) and spectral unmixing was performed using In-Form software (PerkinElmer). Cell segmentation, cell counting, and analysis of marker positivity was performed in an automated manner using QuPath. Color deconvolution was first performed to separate hematoxylin from different markers. Cells were segmented with Stardist,[67] an object detection tool that employs machine learning. To measure whether a cell was positive for a certain marker, an automated method was used with a cutoff value based on the distribution of mean intensities per marker. We assigned a cell to be positive for a marker if the mean intensity was more than 2 standard deviations above the median. Subsequently, we assigned each cell to be Ki67$^+$ only, CD8$^+$ only, CD8$^+$ Ki67$^+$ double-positives or unidentified. For the area measurement, we first used a multilayer perception neural network (MLP) as a pixel classifier in order to differentiate tumor from non-tumor areas. Ten regions per class (tumor, non-tumor) were manually annotated for the training. The tumor regions were then identified on the whole tissue using the pixel classifier. Finally, CD8$^+$Ki67$^+$ double-positive cell densities were computed in tumor areas.

Treatment study

For *in vivo* drug study, formation of T_{RM}-like cells was induced as described above and 5.10^5 kP-OVA were injected 14 days after induction of lung T_{RM}-like cells. Six weeks after tumor cell injection, mice were randomized into isotype controls (Rat IgG2a/Hamster IgG) or anti-PD-1/anti-CTLA-4 (200 mg RMP1-14/150 mg UC10-4F10-11; BioXCell) treatment arms. Two cycles were performed one week apart, each cycle consisting of monoclonal antibody or isotype control administered by intra-peritoneal injection three times over 6 days (day 0, 3, 6). Mice were harvested when they reached ethical endpoint.

Mouse organ preparation for flow cytometry analysis

Left lung lobes were minced and digested in 2 mg/mL collagenase in 0.2% D-glucose in DPBS for 45 min at 37°C. Red blood cells were lysed (0.64% NH_4Cl) and cells were filtered to obtain a single cell suspension before staining for flow cytometry. Spleens were mashed through a sieve followed by red blood cell lysis (0.64% NH_4Cl) and filtration to obtain a single-cell suspension. Livers were mashed through a sieve and cell pellets were resuspended in 35% Percoll (Cytiva, cat # 17089101). Red blood cell lysis was performed (0.64% NH_4Cl) before final filtration to obtain a single-cell suspension. Kidneys were choped and digested in 2 mg/mL collagenase in DPBS for 45 min at 37°C and mashed through a sieve. Cell pellets were resuspended in 44% Percoll and underlayed with 70% Percoll. After centrifugation at 500*g* for 20min, with slow acceleration/brake, the interphase was collected for staining.

Human lung and tumor cell preparation

Lung and tumor samples were either processed immediately or held intact for a maximum of 48 h at 4°C in DMEM/F12 media (Gibco) supplemented with 1 mg/mL of penicillin and streptomycin (Invitrogen). Surgical samples were minced then digested for 1 h at 37°C with 2 mg/mL collagenase I (Worthington, #LS004197) and 200 U/mL deoxyribonuclease (Worthington, #LS002140) in 0.2% D-glucose (Sigma) in DPBS (Gibco), according to our previously published protocols.[5] Samples obtained from EBUS biopsies were digested in collagenase/DNase as above for 45 min. The cell suspension was filtered through a 100 μm cell strainer and washed with 2% FCS-PBS, followed by red blood cell lysis and further washing with 2% FCS-PBS to obtain a single cell suspension. PBMCs were isolated from whole blood using Ficoll-Paque PLUS (GE Healthcare) separation.

Mass cytometry

Single cell suspensions were pulsed for 1 min in 25 μM cisplatin (Sigma Aldrich) at room temperature to label dead cells, washed and then fixed in 1.5% PFA (Electron Microscopy Sciences) for 40 min at RT. Cells were then cryopreserved in cell staining media (CSM, PBS with 0.5% BSA and 0.02% sodium azide) and stored at −80°C. Thawed cells were barcoded using a 20-plex palladium isotope barcoding kit (Fluidigm) according to the manufacturer's directions, blocked with anti-CD16/CD32 FCγ II/III (WEHI antibody facility) and stained with extracellular antibodies for 30 min at RT. Cells were permeabilized at 4°C with methanol for 15 min, washed thrice in CSM, incubated in 100U/mL heparin for 20 min at RT[68] and subsequently stained with antibodies against intracellular markers. Cells were incubated at 4°C with 125 nM $^{191}Ir;^{193}Ir$ DNA intercalator (Fluidigm) in 1.6% PFA overnight and washed in double-distilled water before analysis on a Helios CyTOF (Fluidigm, maintained by Materials Characterisation and Fabrication Plat-form, University of Melbourne). Antibody conjugates that could not be purchased were created from carrier-free antibody solutions conjugated to custom isotopes (Trace Sciences, Fluidigm) using the Maxpar kit (Fluidigm). Antibodies were validated and titrated to ensure specificity and sensitivity. Patient samples were analyzed in batches, with equal numbers of ES and NS patients per run and the inclusion of two reference controls (PBMC and an EBUS metastatic lymph node biopsy) per run to detect batch-to-batch variability.

Analysis of mass cytometry data

All.fcs files generated were concatenated, normalized to beads and debarcoded using the R package Catalyst[69] or Premessa. $CD4^+$ and $CD8^+$ T cells were combined across patients and subjected to viSNE[70] analyzes using CytoBank software. viSNE analyzes were conducted on all phenotyping markers and subject to equal scaling. Samples were also subject to manual gating using reference control samples to standardize between runs (FlowJo) and the R packages limma/pheatmap[71] used to analyze the resulting data.

Flow cytometry

For intracellular staining of mouse and human cells, single cell suspensions were incubated with fixable live/dead GREEN (Invitrogen) or Zombie Aqua (Invitrogen) according to the manufacturer's instructions to distinguish viable cells. Cells were washed with 2%FCS-PBS, blocked with anti-CD16/CD32 FCγ II/III (WEHI antibody facility) and stained with extracellular antibodies for 30 min at 4°C. Cells were fixed and permeabilised with Foxp3/Transcription Factor Staining Kit (eBiosciences) and stained with intracellular antibodies for 30 min at 4°C. Samples were acquired on Aurora spectral unmixing cytometers (CyTEK) and analyzed using Flowjo and Cytobank.

Human lung T cell *in vitro* assays

96-well round bottom plates were coated with 5μg/mL anti-CD3 for a minimum of 2 h at 37°C before rinsing and removing. Human T cells were plated and stimulated with anti-CD3 (OKT3, WEHI monoclonal laboratory, 5 μg/m) and anti-CD28 (BD Biosciences, 1μg/mL) in IMDM media supplemented with 10% fetal calf serum, 1% HEPES, non-essential amino acids, glutamax, sodium pyruvate (all Gibco), 50 μM 2-mercaptoethanol (Sigma) and 100U/mL recombinant IL-2 (Peprotech). Cells were collected for flow cytometry analysis 48 and 72 h after stimulation, Golgi Stop and Golgi Plug (BD) were added to the culture media 3 h before each collection.

Immunohistochemistry and multiplex immunostaining

Human tissue was formalin fixed and paraffin embedded, before antigen retrieval with citrate buffer (10mM, pH 6) and blocking with 10% goat serum. Sections were incubated with antibodies against CD45 for 30 min at RT and stained with biotinylated anti-mouse secondary antibody (Vector Lab) before counterstaining with haematoxylin. Mouse tissue was fixed in 4% paraformaldehyde and paraffin-embedded, before low pH antigen retrieval and staining with primary antibodies and secondary antibody (EnVision+

HRP-rabbit, Dako, catalog #K400311-2) using the EnVision DuoFlex system (Dako). For Dual immunostain, CD8a was detected with DAB (Dako) and Ki67 was detected with Magenta Substrate Chromogen (Dako).

Multiplexed fluorescent IHC with OPAL for CD8 T_{RM} CD39 was performed by sequential staining of a single tissue section with anti-PD-1, anti-CD103, anti-CD69, anti-CD8, anti-panCK and anti-CD39 followed by anti-HRP-mouse and -rabbit secondary antibody and OPAL fluorochrome from OPAL Polaris 7-color manual IHC kit (NEL861001KT). The slides were scanned using the Vectra Polaris microscope (PerkinElmer).

Patient datasets

Access to the TRACERx cohort of 100 NSCLC patients with 327 tumor regions and matched germlines[36] was granted by a Data Access Agreement between the Francis Crick Institute and the Walter and Eliza Hall Institute of Medical Research (DAC #2020-0132). Whole-exome sequencing (WES) alignment files were obtained from the European Genome-phenome Archive (dataset EGAD00001003206). Clinical data and somatic variants were extracted from Tables S2 and S3 in Supplementary Appendix 2 and smoking signatures from Supplementary Appendix 1 of Jamal-Hanjani et al.[36] Variants were converted to standard VCF files for downstream analyzes.

Access to the LxG cohort of 20 lung cancer patients with 39 tumor regions and matched germlines[42] was granted by the Garvan Institute of Medical Research. Whole-genome sequencing (WGS) alignment files, somatic variants, cellularities, smoking signatures and clinical data were obtained from the authors and downloaded from the National Computational Infrastructure of Australia. We excluded 1 patient and 4 tumor regions from analysis due to low cellularity (<20%).

Access to the Chen cohort of pre-invasive (n = 98, adenocarcinoma *in situ* and minimally invasive adenocarcinoma) and invasive LUAD (n = 99) was granted by the FUSCC Chen group. Whole transcriptome (RNA-seq) alignment files were obtained from the European Genome-phenome Archive (dataset EGAD00001005479). Clinical data, TMB, smoking signature percentages and HLA LoH were extracted from the publicly available Source Data of Chen et al.[41]

Access to the Nahar cohort[43] of $EGFR^{mut}$ LUAD (n = 16) was granted by a Data Access Agreement beween the Genome Institute of Singapore, the National Cancer Center of Singapore and the Walter and Eliza Hall Institute of Medical Research. Whole-exome sequencing (WES) alignement files were obtained from the European Genome-phenome Archive (dataset EGAS00001001736).

We used publicly available data from the TCGA cohort of LUAD,[7] using TMB calculated from Hoadley et al[72] and neoantigens from Rooney et al.[73] Clinical data, including smoking status, was downloaded from the Genomic Data Commons website (https://portal.gdc.cancer.gov/projects/TCGA-LUAD).

Tumor mutational burden

Tumor mutational burden (TMB) was calculated for all samples in the LxG and TRACERx by dividing the number of somatic variants passing variant caller quality thresholds by the total capturable area (3,200Mb for LxG and 50Mb for TRACERx).

T_{RM}-like cell signature score in RNA-seq data

Immune infiltration by T_{RM} cells was determined for the TCGA LUAD, and TRACERx cohorts where RNA-seq data were available. featureCounts (v1.6.3)[74] was used on BAM files to obtain read counts per gene for the TRACERx and Chen cohorts. RUV-III was used to remove unwanted variation arising from library size, purity and/or batches from gene counts in all three cohorts.[75] Genes up and down-regulated in T_{RM}-like cells in lung tumor tissue[35] were applied to the normalized gene counts using singscore (v1.12.0)[76] to produce a T_{RM} signature score for each sample indicative of the amount of T_{RM} cells present.

HLA typing and LOH calling

Haplotyping of *HLA-A*, *HLA-B* and *HLA-C* was carried out on all germline and tumor samples in both cohorts using POLYSOLVER (v4) with default parameters.[77] Loss of heterozygosity (LOH) was inferred for each patient by comparing HLA types in tumor samples against the germline type at the resolution of allotype and subtype (2 sets of digits). POLYSOLVER allowed for the analysis of LOH in both WES and WGS datasets. The loss of at least one allele classified the sample as affected by HLA LOH. Clonal LOH was called when an allele was lost in all samples for a patient.

QUANTIFICATION AND STATISTICAL ANALYSIS

Statistical analyzes were run on GraphPad Prism.

Statistical details of experiments can be found in the figure legends and include the statistical tests used, how significance was defined, exact value of n, what n represents, definition of center, and dispersion (mean ± SEM).

For Mass Cytometry analysis, patient samples were analyzed in batches, with equal numbers of ES and NS patients per run and the inclusion of two reference controls (PBMC and an EBUS metastatic lymph node biopsy) per run to detect batch-to-batch variability. For flow cytometry and mass cytometry, data were excluded if < 50 events were counted in a cellular subset.